

POSTPRINT

QUATERNARY SCIENCE REVIEWS

doi:[10.1016/j.quascirev.2021.107245](https://doi.org/10.1016/j.quascirev.2021.107245)

Nonlinear time series analysis of palaeoclimate proxy records

Norbert Marwan^{a,b}, Jonathan F. Donges^{a,c}, Reik V. Donner^{a,d}, Deniz Eroglu^e

^aPotsdam Institute for Climate Impact Research (PIK), Member of the Leibniz Association, Telegrafenberg A31, 14473 Potsdam, Germany

^bInstitute of Geosciences, University of Potsdam, Karl-Liebknecht-Straße 24-25, 14476 Potsdam-Golm, Germany

^cStockholm Resilience Centre, Stockholm University, Kräftriket 2B, 11419 Stockholm, Sweden

^dDepartment of Water, Environment, Construction and Safety, Magdeburg-Stendal University of Applied Sciences, Breitscheidstraße 2, 39114 Magdeburg, Germany

^eFaculty of Engineering and Natural Sciences, Kadir Has University, 34083 Istanbul, Turkey

Nonlinear time series analysis of palaeoclimate proxy records

Norbert Marwan^{a,b}, Jonathan F. Donges^{a,c}, Reik V. Donner^{a,d}, Deniz Eroglu^e

^a*Potsdam Institute for Climate Impact Research (PIK), Member of the Leibniz Association, Telegrafenberg A31, 14473 Potsdam, Germany*

^b*Institute of Geosciences, University of Potsdam, Karl-Liebknecht-Straße 24-25, 14476 Potsdam-Golm, Germany*

^c*Stockholm Resilience Centre, Stockholm University, Kräftriket 2B, 11419 Stockholm, Sweden*

^d*Department of Water, Environment, Construction and Safety, Magdeburg-Stendal University of Applied Sciences, Breitscheidstraße 2, 39114 Magdeburg, Germany*

^e*Faculty of Engineering and Natural Sciences, Kadir Has University, 34083 Istanbul, Turkey*

Abstract

Identifying and characterising dynamical regime shifts, critical transitions or potential tipping points in palaeoclimate time series is relevant for improving the understanding of often highly nonlinear Earth system dynamics. Beyond linear changes in time series properties such as mean, variance, or trend, these nonlinear regime shifts can manifest as changes in signal predictability, regularity, complexity, or higher-order stochastic properties such as multi-stability. In recent years, several classes of methods have been put forward to study these critical transitions in time series data that are based on concepts from nonlinear dynamics, complex systems science, information theory, and stochastic analysis. These include approaches such as phase space-based recurrence plots and recurrence networks, visibility graphs, order pattern-based entropies, and stochastic modelling. Here, we review and compare in detail several prominent methods from these fields by applying them to the same set of marine palaeoclimate proxy records of African climate variations during the past 5 million years. Applying these methods, we observe notable nonlinear transitions in palaeoclimate dynamics in these marine proxy records and discuss them in the context of important climate events and regimes such as phases of intensified Walker circulation, marine

isotope stage M2, the onset of northern hemisphere glaciation and the mid-Pleistocene transition. We find that the studied approaches complement each other by allowing us to point out distinct aspects of dynamical regime shifts in palaeoclimate time series. We also detect significant correlations of these nonlinear regime shift indicators with variations of Earth's orbit, suggesting the latter as potential triggers of nonlinear transitions in palaeoclimate. Overall, the presented study underlines the potentials of nonlinear time series analysis approaches to provide complementary information on dynamical regime shifts in palaeoclimate and their driving processes that cannot be revealed by linear statistics or eyeball inspection of the data alone.

Keywords: nonlinear time series analysis, palaeoclimate proxy, Pliocene, Pleistocene, climate transition, regime shift

1. Introduction

Past climate conditions, variability, and transitions are essential to understand current and future climate changes. In particular, the Plio-Pleistocene can be used as an analogue of future greenhouse climate and how and which regime shifts in large-scale atmospheric and ocean circulation can be expected in a warming world (Burke et al., 2018; Steffen et al., 2018). Moreover, it has been a period of important steps in human evolution, where significant climate regime shifts have most likely influenced the evolution and the migration of human ancestors (deMenocal, 1995; Potts, 1996; DeMenocal, 2004; Trauth, 2005; Staubwasser and Weiss, 2006; Donges et al., 2011b). A better understanding of abrupt climate changes, the pattern of variations, long-distance interrelationships, feedback loops, or the type of dynamics can further help to build our picture of the world and improve corresponding modelling approaches.

The last decades have shown an increasing availability and progress of quantitative approaches in geosciences, ranging from provenance analysis, over rock magnetic measurements, X-ray fluorescence analysis, to isotope geochemistry. Such quantitative approaches have enriched the qualitative studies significantly and allowed new insights that would not have been able to get without them (Sauramo, 1918; Stanley, 1978; Haug and Tiedemann, 1998; Trauth et al., 2021). Most quantitative analysis is traditionally focusing on linear methods of statistics and time series analysis (such as correlations, power spectra, regression analysis, detection of breakpoints, etc.; Trauth

24 (2021); Mudelsee and Stattegger (1997)) as well as partially on extensions
25 thereof (e.g., time-frequency decomposition employing continuous wavelet
26 transforms, Bayesian approaches to breakpoint detection and regression re-
27 placing classical maximum likelihood or least squares estimators (e.g. Schütz
28 and Holschneider, 2011)). Such analyses provide important information on
29 the levels displayed by certain proxy variables and, thus, allow tracing long-
30 term changes of time-average environmental and climatic conditions. How-
31 ever, their application potential can be limited by the fact that real world
32 systems usually consist of many interacting components with feedbacks and
33 nonlinear interrelationships, behave in a more chaotic rather than periodic
34 way, vary in a fashion that cannot be described by a normal distribution
35 (Schölzel and Friederichs, 2008), exhibit distinct behaviours in terms of their
36 extreme event statistics (Albeverio et al., 2006), or represent critical tran-
37 sitions to qualitatively different dynamical regimes (such as tipping points)
38 (Lenton et al., 2008; Schellnhuber, 2009). Concepts from complex systems
39 science, complex networks, and nonlinear dynamics are more appropriate for
40 such problems (Boers et al., 2021; Fan et al., 2021). In the light of the critical
41 impacts of climate and environmental changes on human societies, quantita-
42 tive investigations of large-scale regime shifts (Rocha et al., 2018; Boers and
43 Rypdal, 2021), early warning indicators of such shifts (Dakos et al., 2008;
44 Scheffer et al., 2009; Boettner et al., 2021), and short-term ecosystem re-
45 sponses (Scheffer and Carpenter, 2003; Prasad et al., 2020) on the base of
46 palaeoclimate archives are required. Such insights on critical regime shifts
47 and other large-scale nonlinear changes in Earth system dynamics are highly
48 relevant for determining planetary boundaries delineating a safe operating
49 space that allows for sustainable development of human societies in the An-
50 thropocene (Rockström et al., 2009; Hughes et al., 2013; Steffen et al., 2015).

51 In this study, we review and discuss a selection of data analysis methods
52 that have been widely applied to study complex systems and have their
53 origin in nonlinear dynamics, stochastic modelling, and information theory
54 to identify regime shifts of the palaeoclimate dynamics. While there are
55 many more methods of nonlinear data analysis or machine learning that
56 could be applied in principle, we focus here only on a selection that might be
57 of particular interest for the palaeoclimate researcher when studying regime
58 transitions. After a brief look at linear methods, we will first introduce
59 concepts of nonlinear methods before demonstrating their abilities on marine
60 palaeoclimate records that represent the Plio-Pleistocene climate variation on
61 the northern African continent.

62 2. Methods

63 A plethora of quantitative methods to study palaeoclimate processes have
64 been developed and are available for different purposes. This includes linear
65 and nonlinear methods, or methods using frequentist and Bayesian inference.
66 The selection of the appropriate method depends, of course, on the specific
67 research question.

68 Transitions in climate records can occur at different levels. Related to
69 the time scale, the signal can change abruptly, such as the global temper-
70 ature after an asteroid impact (Brugger et al., 2017), or gradually, such as
71 the slower glaciation (compared to the abrupt warming during the intersta-
72 dials) during the stadials of the glaciation (Dansgaard et al., 1993). We
73 can consider changes of the statistical moments of the time series, such as
74 a change in the mean value (e.g., changing global temperature; Westerhold
75 et al. (2020)) and the variance, or even in higher moments (e.g., skewness
76 of the amplitude distribution). Gradual changes of the signal’s mean cor-
77 respond to trends and are commonly studied by ramp fit models (Mudelsee
78 and Schulz, 1997). More subtle changes in the underlying dynamics can be
79 even more interesting, because they are usually not so obviously visible in
80 the time series, like a change in the mean or variance. For example, the
81 period of a cyclical climate variation can change, as it was found for the mid-
82 Pleistocene transition (MPT) with a shift from a 41 ka to 100 ka climate
83 cycle (Clark et al., 2006). With respect to tipping points, the autocorrela-
84 tion within the signal can be of additional benefit, indicating early warnings
85 of critical climate transitions (such as during the Cenozoic climate (Boettner
86 et al., 2021)). When considering the climate as a dynamical system, it might
87 also be of interest to determine the dimension of the system (i.e., how many
88 differential equations would be necessary to describe the observed dynamics)
89 or whether the system’s dynamics can be characterised as a stochastic, pe-
90 riodic, or chaotic process. Albeit the latter type of behavior corresponds to
91 a deterministic process (which means that its states can be computed), it is
92 difficult to predict.

93 Transitions in climate records based on changes of first statistical mo-
94 ments, trends or periodicity can be analysed with linear methods. For ex-
95 ample, to statistically identify transitions of mean and variance, a running
96 Mann-Whitney or Ansari-Bradley test can be used (Trauth et al., 2009).
97 Regression-based models (Mudelsee and Schulz, 1997) and Bayesian change
98 point detection (Schütz and Holschneider, 2011) are further suitable tools

99 for this research question. Changes in the cyclicities can be analysed with
100 evolutionary power spectra (Trauth, 2021) or with wavelet analysis (Lisiecki,
101 2010). Further developments consider decompositions of the palaeoclimate
102 time series using wavelet transform or singular spectrum analysis (Vautard
103 and Ghil, 1989; Ghil, 2002).

104 Following the progress in nonlinear dynamics and complexity science in
105 the 1970s and 1980s, additional and novel concepts have found their way
106 into Earth sciences. Fractal dimensions and Lyapunov exponents have been
107 promising ideas to better understand, model, and predict the climate sys-
108 tem. However, after a first euphoria, it became clear that palaeoclimate
109 data, in particular, comes with problems that make it almost impossible to
110 apply such methods reliably (Grassberger, 1986; Maasch, 1989; Schulz et al.,
111 1994): the data is non-stationary, the sampling is irregular, the uncertainties
112 are too high due to dating uncertainties, many degrees of freedom, and bad
113 signal-to-noise ratio. Despite the problems with some methods, other meth-
114 ods were more successful, such as the already mentioned singular spectrum
115 analysis (Vautard and Ghil, 1989), potential analysis (Livina et al., 2010),
116 or recurrence analysis (Marwan et al., 2007). In the following, we will focus
117 on selected methods based on concepts of complex systems and nonlinear
118 dynamics that can be used to study different aspects of transitions in palaeo-
119 climate dynamics (see Tab. 1). We will also add information about available
120 software packages. The corresponding links to the software can be found in
121 the Appendix.

122 *2.1. Windowing approach*

123 The detection of transitions in the dynamics is based on the idea that
124 some statistical properties change with time. To evaluate such changes, we
125 have to calculate a certain quantity or measure at a certain point in time
126 and compare it with previous or later values of this quantity. Most of the
127 quantities need, however, a larger number of values to be calculated, i.e., we
128 need to divide our time series into short pieces or time windows of length w .
129 Such a time window is then moved over the entire time series. The window
130 has a starting point t_1 , an endpoint t_2 , and a center point $(t_2 - t_1)/2$. The
131 quantity calculated within this window is then assigned to this centre point
132 and, thus, provides a new time series of this quantity. The moving step of
133 this window ws sets the temporal resolution of the new quantity time series.
134 However, the smaller ws , the larger the overlap and the more redundant the
135 information of subsequent quantity values. We have, therefore, to find a good

136 trade-off between redundant information and temporal resolution. A change
 137 of this quantity over time can then be interpreted concerning the investigated
 138 regime transition. Moreover, we have to consider the window size when
 139 interpreting the results. For example, using a time window of length 410 ka,
 140 an abrupt increase of a transition measure at 2 Ma before present (BP) would
 141 mean that the transition happened not earlier than approximately 1.795 Ma
 142 BP (because of the used centre point of the window). A single point covers
 143 a period of 410 ka; for a used offset of 41 ka, two consecutive points of time
 144 correspond to 410 + 41 ka, and so on.

145 2.2. Statistical mechanics and information theory

146 *Complexity* is a concept that characterizes the dynamical behaviour of
 147 a given complex system whose many parts interact in many different ways.
 148 Complex behaviour (and chaotic dynamics) usually appear in nonlinear sys-
 149 tems and can be measured with various complexity measures. One of the
 150 most well-known complexity measures is the entropy (a measure of informa-
 151 tion theory), which measures the uncertainty in a system (Shannon, 1948).
 152 The entropy measure has been used to detect abrupt changes and regime
 153 transitions from data in different disciplines such as life sciences, engineer-
 154 ing, economics, and Earth sciences (Gapelyuk et al., 2010; Li et al., 2013;
 155 Afsar et al., 2016; Zhao et al., 2020).

156 *Shannon entropy.* For a given time series $x(t)$, the Shannon entropy S is
 157 defined as

$$S = - \sum_x \rho(x) \log \rho(x), \quad (1)$$

158 where $\rho(x)$ is the probability density function (PDF) of the values x of the
 159 time series (in practice, this is approximated by n discrete bins i , with h_i
 160 the probability that the time series value x falls within the interval i and
 161 $S = - \sum_i^n h_i \log h_i$). The PDF is a function that specifies the probability of
 162 a randomly picked point from the observation $x(t)$ existing within a particular
 163 interval (range of values). As an intuitive point of view, if the probabilities
 164 are approximately the same for each specified interval (i.e., when having a
 165 homogenous probability distribution), the entropy is expected to be high
 166 since the randomly picked point can be in one of the intervals with equal
 167 probability. In other words, there is no way to find an interval in which a
 168 randomly chosen number would be drawn with high probability. Contrarily,
 169 if the distribution is heterogeneous, then the entropy is expected to be low

170 and we will be much less uncertain in predicting a random pick from the
 171 data (Fig. 1). Hence, the Shannon entropy defined solely on individual time
 172 series data is a purely distributional property. Nevertheless, a change of the
 173 entropy over time can be used to identify exceptional states, an application
 174 that is used, e.g., to detect intense magnetic storms (Balasis et al., 2008).

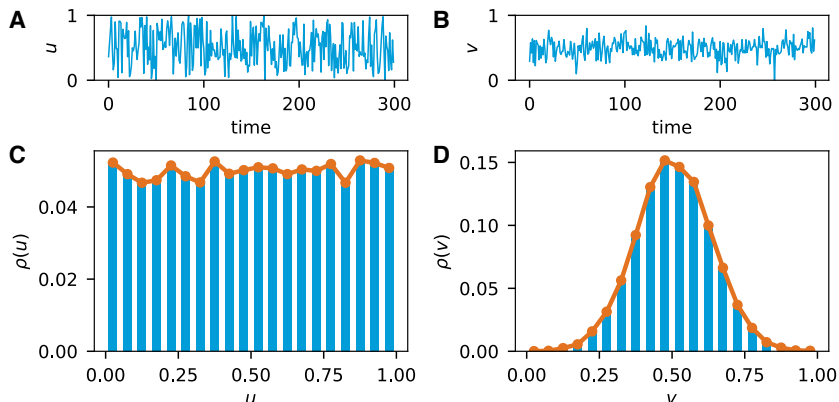


Figure 1: Illustration of (A, B) random time series u and v and (C, D) their probability density functions $\rho(u)$ and $\rho(v)$. The entropy of (A, C) u with uniform distribution is $S_u \approx 3.0$ and (B, D) v with normal distribution is $S_v \approx 2.37$.

175 Simple PDF dependent statistical measures like Shannon entropy do not
 176 consider the order of samplings, i.e., they neglect deterministic changes in the
 177 data. Therefore, we have to be careful in interpreting the Shannon entropy
 178 value calculated directly from the data with respect to the complexity of the
 179 dynamics (Fig. 2).

180 In order to incorporate different aspects of the data, such as the dynamics,
 181 various concepts and approaches have been developed for the construction of
 182 a suitable PDF. These different procedures led to various entropy measures
 183 such as the Tsallis entropy, order (permutation) entropy, and block entropy
 184 (Balasis et al., 2013; Boaretto et al., 2021). Further and more advanced
 185 information based measures, derived from the dynamical systems theory,
 186 are, e.g., Kolmogorov-Sinai entropy or correlation entropy (Grassberger and
 187 Procaccia, 1984).

188 *Order Entropy (Permutation Entropy)*. As mentioned above, changing the
 189 order of the numbers in a time series does not change the value of the Shannon
 190 entropy. Dynamically different systems can have very similar PDFs and,
 191 therefore, similar entropy values due to order ignorance (Fig. 2).

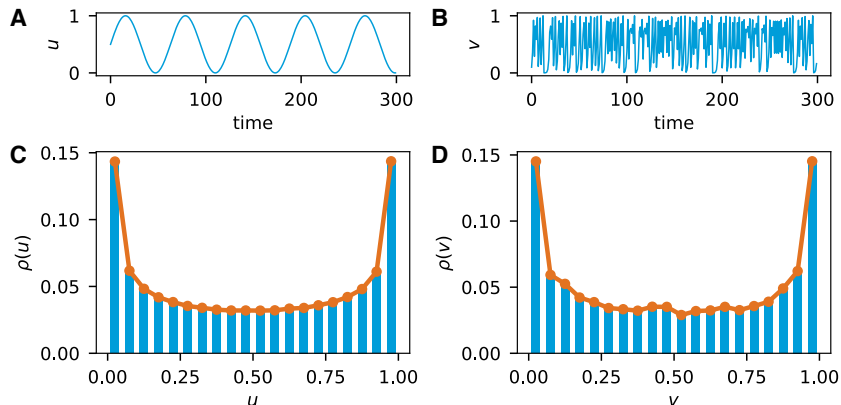


Figure 2: Entropy measures can fail detecting different dynamical regimes, as such of (A) a sinusoidal wave u and (B) a chaotic signal (generated using logistic map $v(t + 1) = 4v(t)(1 - v(t))$). Although the dynamics represented by u and v is entirely different, the (C, D) PDFs are similar. Therefore, the entropy of u and v are $S_u \approx S_v \approx 2.84$.

192 To take into account the dynamics of the system, short sequences of
 193 the time series have to be considered. A simple approach for such is to
 194 consider the local rank order of subsequent values of the time series (Zanin
 195 and Olivares, 2021). Such order pattern reduces the value range to only a few
 196 numbers and encodes the dynamical behaviour. For calculating the entropy,
 197 the PDF of the order patterns is used.

198 In the simplest case (pattern of order two, $d = 2$), a time series (x_1, x_2, \dots, x_N)
 199 can be discretized by comparing the values at two time points

$$\pi_i = \begin{cases} 0 & x_i < x_{i+\tau}, \\ 1 & x_i > x_{i+\tau}, \end{cases} \quad (2)$$

200 where τ is a delay parameter that allows some adjustment to a time scale of
 201 interest (such as the typical period of a cyclic signal). In the present study,
 202 we use order patterns of degree $d = 3$, providing six different order patterns
 203 (Fig. 3). A degree of $d = 3$ is usually sufficient to describe the important
 204 dynamical properties of the time series (Bandt and Shiha, 2007). Moreover,
 205 the number of possible order patterns is $d!$. In order to estimate a reliable
 206 PDF of the $d!$ different order patterns, we need longer and longer time series
 207 for larger d , which are often not available in real applications.

208 Then, the order (or permutation) entropy is the Shannon entropy of the

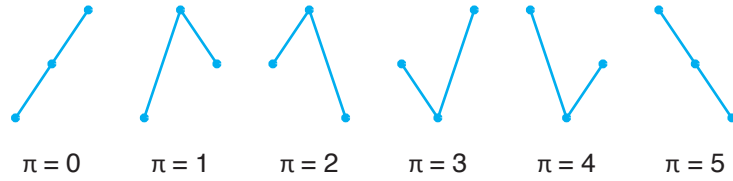


Figure 3: Order patterns of dimension $d = 3$.

209 PDF of the order patterns

$$S_{\text{order}} = - \sum_{i=1}^{d!} \rho(\pi_i) \log \rho(\pi_i). \quad (3)$$

210 Such entropy measure enables us to detect different dynamical regimes
 211 (Boaretto et al., 2021), because some dynamics is related to a tendency to cer-
 212 tain order patterns (e.g., periodic dynamics), where others can lead to more
 213 equally frequent order patterns (e.g., stochastic dynamics; Fig. 4). Because
 214 it does not characterize the PDF of the amplitude distribution, processes
 215 with the same dynamics but different PDF cannot be distinguished (Fig. 5).
 216 Thus, the use of the Shannon entropy and the order entropy depends on
 217 the research question, i.e., whether we need to characterize the amplitude
 218 distribution or the dynamics.

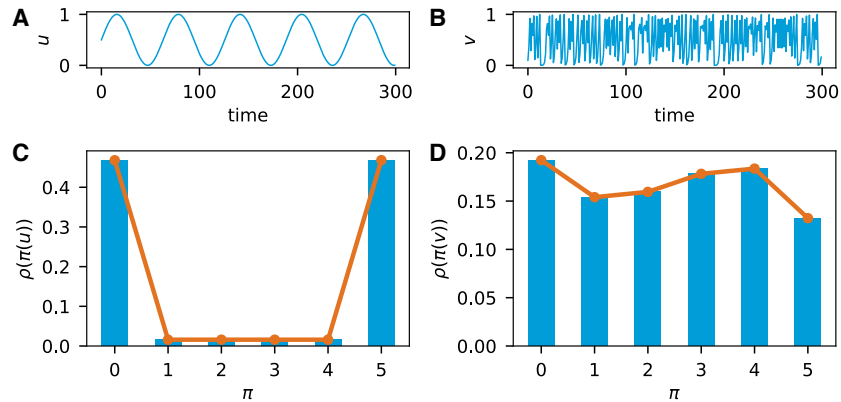


Figure 4: In contrast to the Shannon entropy, the order (permutation) entropy ($d = 3$) detects different dynamical regimes, such as (A) a sinusoidal signal u and (B) a chaotic signal (generated using logistic map $v(t+1) = 4v(t)(1-v(t))$). Although the PDF of time series are similar (see Fig. 2), the PDF of order patterns differ from each other (C, D) and the order entropy of u and v differs clearly, $S_{\text{order}}(u) \approx 0.98$ and $S_{\text{order}}(v) \approx 1.78$.

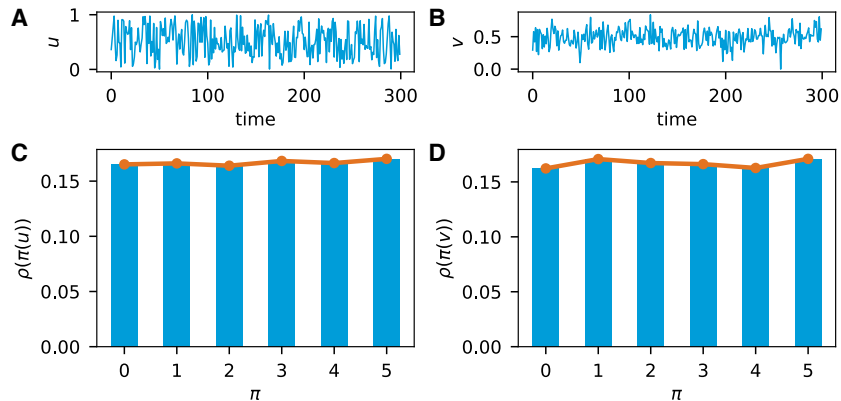


Figure 5: Illustration of (A, B) white noise u and v with different PDFs $\rho(u)$ and $\rho(v)$, but similar PDFs of the order patterns (C, D). The order entropy does not distinguish between these two random processes: $S_u \approx 1.79$ and $S_v \approx 1.79$.

219 Order entropy can be a useful measure to check anomalies in the data or
 220 to identify such segments that are not associated with the climatic processes
 221 of interest (Garland et al., 2018). It has also been used to detect periodic
 222 changes in climate proxies of the late Silurian and to establish a corresponding
 223 astrochronology (Spiridonov et al., 2020).

224 *Confidence intervals.* Applying the windowing approach, the entropy mea-
 225 sures are changing over time. We might ask, how significant such variation
 226 is. To assess the significance, we consider a null-hypothesis of “no temporal
 227 change” in the considered characteristic of the time series, given the proper-
 228 ties of this time series. Unfortunately, for nonlinear data analysis, no general
 229 significance test is available with tables and significance values in textbooks.
 230 Therefore, we have to create the test individually, incorporating the specific
 231 settings and conditions given by the research question. To test the above
 232 null-hypothesis, we use the original time series to create artificial time series
 233 which comply with the specific null-hypothesis. Such time series are also
 234 called surrogates. We can create such surrogate time series by bootstrapping
 235 values from the original time series. The entropy measure is then calculated
 236 from the surrogate. By repeating this procedure many times, we get an em-
 237 pirical test distribution of the entropy measure, which represents the entropy
 238 values to be expected under the null-hypothesis. Now, we can use the 5% and
 239 95%-quantiles of this test distribution to define a two-sided 90%-confidence
 240 interval. If the entropy measure in a certain window exceeds the confidence

241 interval, we consider this value as significantly different and the dynamics
242 has changed.

243 *Software.* Entropy can be easily calculated from time series by their proba-
244 bility distributions. This measure is often part in larger software solutions,
245 such as in the *CRP Toolbox* for MATLAB (see Appendix for links). For order
246 entropy, specific packages are available, e.g., for Python the *ordpy* package
247 (Pessa and Ribeiro, 2021), or for MATLAB the *Permutation entropy* pack-
248 age.

249 2.3. Stochastic modelling (potential analysis)

250 The behaviour of many dynamical systems can be described by a stochas-
251 tic differential equation, e.g., a changing climate which is forced by a stochas-
252 tic process. The conceptual model for such a process can be described by
253 the simple equation (which is a stochastic differential equation) (Gardiner,
254 2009; Kwasniok and Lohmann, 2009, 2012)

$$\frac{dx}{dt} = -\frac{dU(x)}{dx} + \sigma dW, \quad (4)$$

255 with x corresponding to the slowly changing climate state, $U(x)$ the poten-
256 tial which restricts the possible states x , σ the amplitude of the stochastic
257 process, and W a real valued continuous time stochastic (Wiener) process.
258 The complexity of the potential $U(x)$ determines the number of states, e.g.,
259 for a double-well potential $U(x) = -2x^2 + x^4$ we will find two different states
260 between which the system can jump (Fig. 6A).

261 By exploiting the associated Fokker-Planck equation, we can find the
262 probability density function of the process depending on the potential (Risken,
263 1989):

$$\rho(x) \sim e^{-\frac{2U(x)}{\sigma^2}}. \quad (5)$$

264 The PDF $\rho(x)$ can be estimated from a time series x using a standard Gaus-
265 sian kernel estimator (Silverman, 1986). Thus, we can now find a reconstruc-
266 tion of the potential by (Fig. 6)

$$\hat{U} = -\frac{\sigma^2}{2} \log \rho(x). \quad (6)$$

267 The parameters of the Eq. (4) can also be estimated by more sophisti-
268 cated approaches, such as the Kramers-Moyal or Mori-Zwanzig approaches

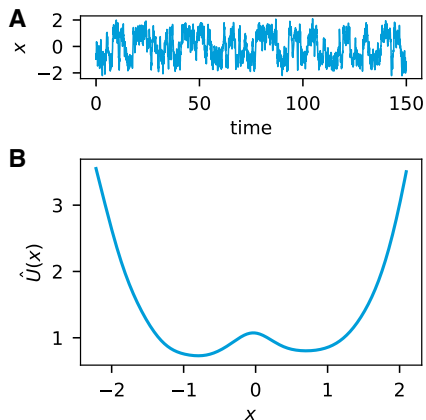


Figure 6: A stochastic process simulated using Eq. (6) with the double-well potential $U(x) = -2x^2 + x^4$. Using the generated random time series x , the potential function $\hat{U}(x)$ is reconstructed. As the double-well potential is considered in the time series generation, we find two wells ($n_U = 2$) in the reconstructed potential function.

269 (Friedrich et al., 2011; Hassanibesheli et al., 2020) or the unscented Kalman
 270 filter (Kwasniok and Lohmann, 2009, 2012), which have been mainly applied
 271 to trace dynamical regime changes (e.g., DO events) in ice core data. How-
 272 ever, for the sake of simplicity, we use here the simple approach using the
 273 PDF estimation.

274 Counting the wells of the reconstructed potential \hat{U} , we have an estimate
 275 of the number of possible states n_U (Livina et al., 2010). This approach was
 276 successfully applied to study the bifurcation behaviour of the climate in the
 277 Pliocene using benthic stable isotope and ice core data (Livina et al., 2010,
 278 2011, 2012).

279 *Software.* For the simple approach of kernel based PDF estimation as used
 280 here, the corresponding functionality is usually already included in many
 281 software packages (e.g., in *scipy* for Python or in the *Statistics and Machine*
 282 *Learning Toolbox* for MATLAB). Parameter estimation using the Kramers-
 283 Moyal approach or the unscented Kalman filter can be performed using the
 284 *kramersmoyal* and *FilterPy* packages for Python.

285 2.4. Phase space-based approaches

286 Dynamical systems theory considers the underlying dynamics of the ob-
 287 served, measured system. The idea is that all n state variables of the dy-
 288 namical system span an n -dimensional space and that a point in such a

289 space corresponds to the state of the system (Fig. 7B). With time, such a
 290 point moves in this phase space and forms a trajectory (the phase space
 291 trajectory). Such a phase space trajectory is the starting point for different
 292 analysis approaches, in particular for many nonlinear measures.

Phase space reconstruction. In many practical situations, only one observ-
 able (i.e., a single time series) is available and the phase space has to be
 reconstructed (Takens, 1981). Several approaches have been suggested for
 phase space reconstruction, using time shifted copies or derivatives (Lekscha
 and Donner, 2018; Kraemer et al., 2021). For the sake of simplicity, here
 we use the widely used approach of time-delay embedding with constant de-
 lays (Packard et al., 1980), where the phase space vector $\vec{x}(t) = \vec{x}_i$ (with
 $t = i\Delta t$ and Δt the sampling time) is formed from one observation $x(t)$ by
 time-shifted copies

$$\vec{x}_i = \left(x_i, x_{i+\tau}, \dots, x_{i+(m-1)\tau} \right),$$

293 with m and τ the embedding dimension and the embedding delay (Figs. 7
 294 and 8B). Under general conditions, the reconstructed phase space can be
 295 considered topologically equivalent to the original phase space. The embed-
 296 ding delay τ has to be chosen in such a way, that a dependence between the
 297 vector components of \vec{x} vanishes. An often used means of determining the
 298 delay is the *autocorrelation function* $C(\tau) = \langle x_i x_{i-\tau} \rangle$ ($\langle x \rangle = 0$, $\sigma(x) = 1$, and
 299 $\langle \cdot \rangle$ denoting the arithmetic mean). A delay may be appropriate when the
 300 autocorrelation approaches zero for this value of delay or at least falls below
 301 a certain de-correlation threshold (corresponding to the autocorrelation time
 302 τ_c , which is where $C(\tau_c) \approx 1/e$) (Kantz and Schreiber, 1997), minimizing
 303 the linear correlation between the components (absence of linear correlation
 304 does not mean necessarily statistical independence in general, but only linear
 305 independence).

306 A practically efficient and widely used approach for the determination
 307 of the smallest sufficient embedding dimension m uses the number of *false*
 308 *nearest neighbors*. The basic idea is that by decreasing the embedding dimen-
 309 sion an increasing amount of phase space points will be projected into the
 310 neighbourhood of any phase space point, even if they are not real neighbours.
 311 Such points are called *false nearest neighbours* (FNNs). The simplest method
 312 uses the amount of these FNNs as a function of the embedding dimension
 313 in order to find the minimal embedding dimension (Kantz and Schreiber,

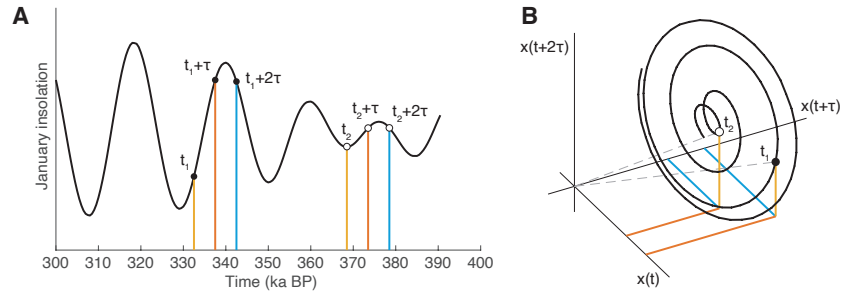


Figure 7: Illustration of the phase space reconstruction of (A) a time series (January insolation at latitude 20°N) by time-delay embedding (B). A state at time t_1 is constructed from time series values that are shifted by a small delay τ (black points in A) which serve as the coordinates in the phase space (B). Black points correspond to time t_1 and white points to time t_2 .

314 1997). Such a dimension has to be taken where the FNNs vanish. Additional
 315 criteria could be applied, e.g., the ratios of the distances between the same
 316 neighbouring points for different dimensions (Kennel et al., 1992; Cao, 1997;
 317 Kraemer et al., 2021).

318 *Phase space properties.* A classical approach of analyzing the phase space is
 319 the estimation of the correlation dimension and general fractal dimensions
 320 (Grassberger and Procaccia, 1983). Whereas the integer part of the dimen-
 321 sion can give some hint on the degree of freedom of the dynamical system (i.e.,
 322 how many variables we would need to describe such a dynamics), a possible
 323 fractional part of the dimension value is considered to be of special interest,
 324 because it means that the phase space trajectory has fractal properties and
 325 the dynamics is rather irregular. However, despite the initial euphoria and
 326 the estimations of the fractal dimension from numerous geophysical data sets,
 327 it finally turned out that this measure is often too sensitive to the amount
 328 of noise typical for this kind of data (Maasch, 1989; Schulz et al., 1994).
 329 Moreover, the initial requirement of long and stationary records can also not
 330 be sophisticated by the usually available data (Eckmann and Ruelle, 1992).
 331 Estimations of fractal dimensions from real world data have been, therefore,
 332 controversial (e.g., Grassberger, 1986; Möller et al., 1989; Gershenfeld, 1992).

333 Another fundamental property of interest of the phase space trajectory is
 334 its divergence behaviour. Tiny displacements in the phase space can result
 335 in heavily diverging trajectories, i.e., to completely different states. In such
 336 cases, we refer to this as a chaotic behaviour, because the states depend

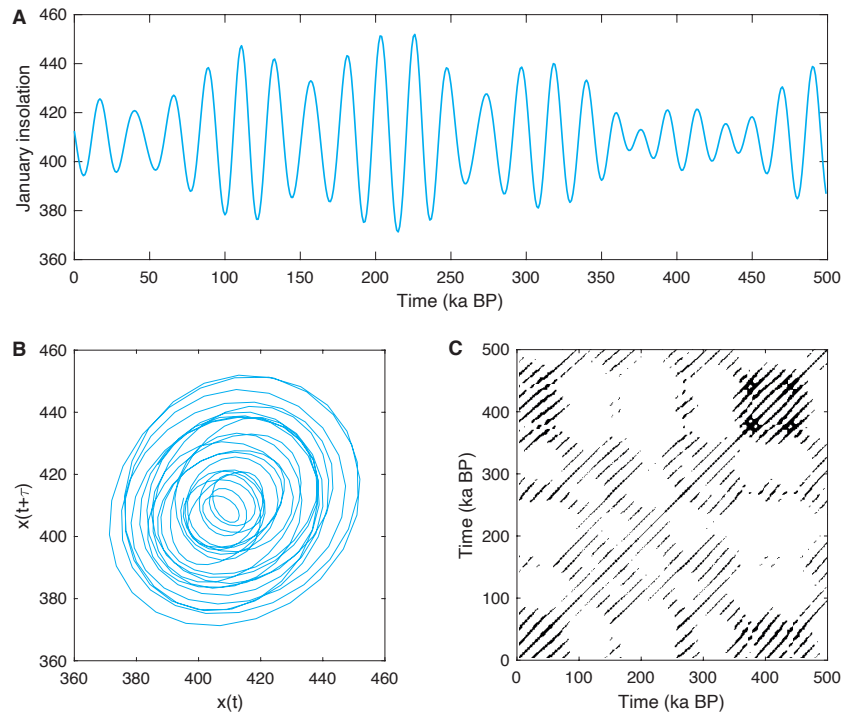


Figure 8: (A) January insolation at latitude 20°N for the last 500 ka as an exemplary time series to illustrate the phase space and recurrence plot approach. (B) Phase space representation of the insolation time series in (A) based on a time delay embedding using a delay of $\tau = 6$ ka and embedding dimension $m = 2$. (C) Recurrence plot of the insolation time series; the recurrence threshold $\varepsilon = 10$. The cyclical variations are visible by the periodic diagonal lines in the recurrence plot.

337 strongly on the initial conditions and are not predictable. The diverging of
 338 the trajectory due to small deviations in initial values is measured by the
 339 Lyapunov exponent (Wolf et al., 1985; Kantz, 1994). Positive values indicate
 340 chaotic dynamics. But similar to the estimation of fractal dimensions, a
 341 reliable estimation of the Lyapunov exponent requires also long time series
 342 (Eckmann and Ruelle, 1992). If only the largest Lyapunov exponent is of
 343 interest, several approximating approaches have been suggested (Kantz, 1994;
 344 Rosenstein et al., 1993).

345 *Recurrence plots.* A more recent approach of analyzing complex dynamics
 346 by the phase space trajectory is by investigating its recurrence behaviour.
 347 A powerful framework for recurrence analysis is provided by the recurrence
 348 plot (RP) (Marwan et al., 2007). A RP represents all such time points j
 349 which a state \vec{x}_i recurs:

$$R_{i,j} = \begin{cases} 1 & \text{if } \vec{x}_i \approx \vec{x}_j, \\ 0 & \text{otherwise.} \end{cases} \quad (7)$$

350 The recurrence of a state is usually defined by the closeness of two states,
 351 measured by comparing their spatial distance $D_{i,j} = \|\vec{x}_i - \vec{x}_j\|$ with a thresh-
 352 old ε :

$$R_{i,j} = \Theta(\varepsilon - D_{i,j}), \quad (8)$$

353 with Θ the Heaviside function ($\Theta(x < 0) = 0$, $\Theta(x \geq 0) = 1$). Different
 354 research questions and applications can require different recurrence defini-
 355 tions (Marwan et al., 2007). Here we use one based on Euclidean norm
 356 and selecting a threshold ε to ensure a predefined recurrence point density,
 357 $RR = N^{-2} \sum_{ij} R_{i,j}$ (Kraemer et al., 2018). The resulting recurrence matrix
 358 \mathbf{R} is a $N \times N$ binary matrix (with N the number of considered states, i.e.,
 359 time points).

360 *Recurrence quantification analysis.* Although the RP is a visualization tech-
 361 nique for recurrences in phase space, it is the base for different recurrence
 362 quantification approaches. By looking at a RP (Fig. 8C), we identify some
 363 characteristic features: lines that are parallel to the main diagonal and some
 364 vertically extended block structures (vertical lines). The presence of diagonal
 365 and vertical lines reflects the dynamics of the system and is related to diver-
 366 gence (Lyapunov exponents) and intermittency (Marwan et al., 2002; Thiel
 367 et al., 2004; Marwan et al., 2007). Following a heuristic approach, a quanti-
 368 tative description of RPs based on these line structures was introduced and is

369 known as recurrence quantification analysis (RQA) (Zbilut and Webber, Jr.,
 370 2007; Marwan, 2008) that has demonstrated its power and potential in nu-
 371 merous scientific disciplines for various applications. It can be used to study
 372 regime changes, dynamical transitions, characterizing dynamics, classifying
 373 different dynamical behaviour, detecting synchronization, and coupling di-
 374 rections (Marwan et al., 2007; Marwan, 2008; Webber, Jr. et al., 2009). For
 375 palaeoclimate research, it is a promising tool to identify climate transitions,
 376 such as the Cenozoic climate regimes of hothouse, warmhouse, coolhouse,
 377 and coldhouse states (Westerhold et al., 2020), Pleistocene and Holocene
 378 changes in the Asian monsoon system (Eroglu et al., 2016; Lechleitner et al.,
 379 2017; Goswami et al., 2018; Han et al., 2020) African climate (Trauth et al.,
 380 2021) and El Niño/ Southern Oscillation activity (Marwan et al., 2003),
 381 Holocene vegetation patterns and environmental changes (Spiridonov et al.,
 382 2019, 2021), or decadal solar variations (Voss et al., 1996). It was also used to
 383 identify global temperature forcing in historical data (Goswami et al., 2013)
 384 and as a test framework in a study on the volcanic impact on the coupling
 385 between El Niño/ Southern Oscillation and Indian Summer monsoon (Singh
 386 et al., 2020).

387 Epochs of the phase space trajectory that evolve in a similar way, i.e., run
 388 close and parallel in the phase space, cause diagonal structures in the RP.
 389 The length of such diagonal line structures depends on the predictability and,
 390 hence, the dynamics of the system (periodic, chaotic, stochastic). Therefore,
 391 the histogram $P(l)$ of diagonal line lengths l is one of the important features
 392 used by several RQA measures for characterizing the system's dynamics.

393 A central RQA measure is quantifying the fraction of recurrence points
 394 $R_{i,j} \equiv 1$ that form diagonal lines:

$$DET = \frac{\sum_{l=l_{\min}}^N l P(l)}{\sum_{l=1}^N l P(l)}. \quad (9)$$

395 This measure is called *determinism* because the relative amount of diagonal
 396 lines vanishes for stochastic, but is high for deterministic processes. We can
 397 use this measure as an indicator of predicability. Here, we use it in a relative
 398 manner, i.e., interpret dynamics of increased DET values as relatively more
 399 predictable than such with lower values. For the definition of a diagonal
 400 line, we use a minimal length l_{\min} that should be of the order of the auto-
 401 correlation time (Marwan et al., 2007).

402 Another RQA measure is quantifying slowly changing states, as occur-
 403 ring during laminar phases (intermittency). Such dynamics result in vertical

404 structures in the RP. Similar to the definition of DET, we can calculate
 405 the fraction of recurrence points forming vertical structures to all recurrence
 406 points,

$$LAM = \frac{\sum_{v=v_{\min}}^N v P(v)}{\sum_{v=1}^N v P(v)}, \quad (10)$$

407 which is called *laminarity* (Marwan et al., 2007). $P(v)$ is the histogram
 408 of vertical lines of length v . Measures based on vertical structures allow
 409 to detect chaos-chaos transitions, whereas measures based on diagonal lines
 410 detect chaos-order transitions. Here we use this measure to evaluate the
 411 persistence of variations relatively.

412 The confidence of the variations in the recurrence measures (using the
 413 moving windows approach) can be determined with a specific, bootstrap
 414 based statistical test (Marwan et al., 2013). For all moving windows s , the
 415 individual distributions of diagonal line lengths $P_s(l)$ are merged $P^*(l) =$
 416 $\sum_s P_s(l)$. From this distribution, line lengths are drawn and used to con-
 417 struct a new individual distribution $\hat{P}_s(l)$, from which we calculate the DET
 418 measure. This bootstrapping of line lengths is repeated many times, produc-
 419 ing a distribution of DET values which correspond to an overall dynamics,
 420 i.e., representing a baseline dynamics. The 5% and 95%-quantiles of this em-
 421 pirical test distribution are then used as the 90%-confidence interval and to
 422 assess the significance of excursions of the DET values over time. A similar
 423 approach is used for the vertical line based measure LAM.

424 *Recurrence networks.* An extension to quantify the recurrences in phase
 425 space is to identify the recurrence matrix \mathbf{R} as a link matrix \mathbf{A} of a net-
 426 work and to use measures from complex network theory (Marwan et al.,
 427 2009; Donner et al., 2010). Excluding self-loops, we obtain \mathbf{A} from the RP
 428 by removing the identity matrix,

$$A_{i,j} = R_{i,j} - \delta_{i,j}, \quad (11)$$

429 where $\delta_{i,j}$ is the Kronecker delta ($\delta_{i,j \neq i} = 0$, $\delta_{i,j=i} = 1$). The resulting un-
 430 weighted and undirected network consists of phase space vectors (associated
 431 with their time points) as nodes and recurrences as links (Fig. 9). A differ-
 432 ence to the recurrence quantification analysis is that in a network the nodes
 433 can be reordered (meaning the temporal sequence is not important) without
 434 changing the network properties, while in recurrence plots and recurrence
 435 quantification analysis the temporal ordering of the states is fundamental.

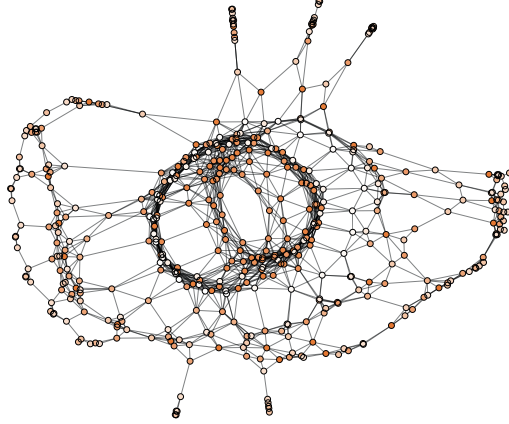


Figure 9: Recurrence network of the insolation time series as shown in Fig. 8A. The colour represents the time (the older the darker the colour).

436 Complex network measures can characterize the network nodes separately
 437 or the entire network as a whole, by local or global measures, e.g., for detect-
 438 ing different dynamical regimes or unstable periodic orbits (Marwan et al.,
 439 2009; Zou et al., 2010; Donner et al., 2011). An important measure is the
 440 *network transitivity*

$$\mathcal{T} = \frac{\sum_{i,j,k=1}^N A_{i,j} A_{j,k} A_{k,i}}{\sum_{i,j,k=1}^N A_{i,j} A_{k,i}}, \quad (12)$$

441 revealing the probability that two neighbours (i.e. recurrences) of any state
 442 are also neighbours (Barrat and Weigt, 2000). Intuitively, dynamics with
 443 fast diverging phase space trajectories will have a rather low probability that
 444 such triangle configurations of connected nodes retain for some time. In
 445 contrast, regular or periodic dynamics will exhibit a high probability of the
 446 occurrence of such triangles. Therefore, high values in \mathcal{T} represent regular
 447 and low values an irregular dynamics (Zou et al., 2010), which is supported
 448 by the interpretation of this measure as being directly linked to a generalized
 449 notion of the effective spatial dimensionality of the network in phase space
 450 (Donner et al., 2011).

451 Another interesting network measure for recurrence analysis is the average
 452 length of shortest paths between all pairs of nodes, the *average path length*

$$\mathcal{L} = \frac{1}{N(N-1)} \sum_{i,j=1}^N \ell_{i,j}, \quad (13)$$

453 where the length of a shortest path $\ell_{i,j}$ is defined as the minimum number
454 of links that have to be crossed to travel from node i to node j (Boccaletti
455 et al., 2006). Disconnected pairs of nodes are not included in the average.

456 The confidence intervals for the network measures are estimated in a
457 similar way as for the entropy measures. We create surrogate time series by
458 bootstrapping values from the time series and calculate the network measures
459 from the corresponding recurrence networks. By repeating this procedure
460 many times, the empirical test distributions are created, which are then used
461 to find the 5% and 95%-quantiles as the confidence interval.

462 The recurrence network approach was used to identify palaeoclimate
463 regime transitions, such as the Plio-Pleistocene African climate variability
464 and its relationship to human evolution (Donges et al., 2011b) or the
465 Holocene variability of the Asian monsoon and its impact on ecosystems
466 (Marwan and Kurths, 2015; Prasad et al., 2020) and ancient human soci-
467 eties (Donges et al., 2015a). Another application was investigating the link
468 between the Indian and the East Asian monsoon (Feldhoff et al., 2012).

469 Further phase space based measures are available and can be useful.
470 These include other RQA and recurrence network measures e.g., trapping
471 time and mean average diagonal line length (Marwan et al., 2002), measures
472 evaluating similarities in phase space such as FLUS (Malik et al., 2014), or
473 entropy estimates, e.g., sample entropy (Richman and Moorman, 2000) or
474 recurrence period density entropy (Little et al., 2007).

475 *Software.* The number of software packages for recurrence analyses is contin-
476 uously increasing due to the increasing popularity of this method. Examples
477 for Python are the *pyunicorn* package (Donges et al., 2015b) or the *PyRQA*
478 package (Rawald et al., 2017), and for MATLAB the *CRP Toolbox* (see Ap-
479 pendix for links).

480 2.5. Visibility graphs

481 An alternative approach to transform time series to networks and to char-
482 acterise them by their network properties is based on visibility graphs, origi-
483 nally introduced for the detection of obstacles by mutual visibility relation-
484 ships between points in two-dimensional landscapes (e.g., for automatisa-
485 tion and architectural design) (Lacasa et al., 2008). Similar to recurrence net-
486 works, a network node represents a time point. A link $A_{ij} = 1$ is now defined
487 by the rule

$$\frac{x_i - x_k}{t_k - t_i} > \frac{x_i - x_j}{t_j - t_i} \quad (14)$$

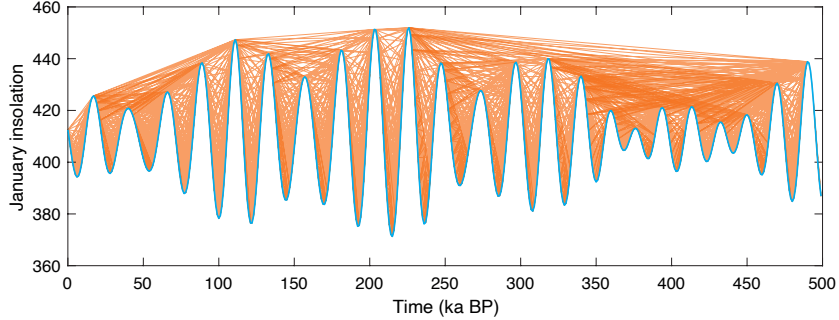


Figure 10: Visibility graph of the insolation time series as shown in Fig. 8A.

488 for all time points t_k with $t_i < t_k < t_j$, i.e., we can connect the values at t_i
 489 and t_j by a straight line without crossing another local peak in between them
 490 (Fig. 10). The topology of the visibility networks is related with fractal and
 491 multifractal properties of the underlying time series (Lacasa et al., 2009).

492 Another, even more interesting application of visibility networks is their
 493 ability to identify time irreversibility in time series. Time irreversibility is
 494 a typical indicator of nonlinear dynamics (Theiler et al., 1992). Visibility
 495 networks can be used to test for this specific type of dynamics, in particular
 496 to identify nonlinear regime shifts (Lacasa et al., 2012; Donges et al., 2013).

497 The basic idea is to compare the statistics of links coming from the past
 498 ($A_{j<i}$) or going into the future ($A_{j>i}$), referred to as retarded and advanced
 499 links (in the visibility network all links have a clear time direction). We can
 500 use the retarded and advanced degrees

$$k_i^r = \sum_{j<i} A_{ij}, \quad k_i^a = \sum_{j>i} A_{ij}, \quad (15)$$

501 with $k_i = k_i^r + k_i^a$, or the clustering coefficient of the advanced and retarded
 502 links

$$\begin{aligned} \mathcal{C}_i^r &= \binom{k_i^r}{2}^{-1} \sum_{j<i, k<i} A_{ij} A_{jk} A_{ki}, \\ \mathcal{C}_i^a &= \binom{k_i^a}{2}^{-1} \sum_{j>i, k>i} A_{ij} A_{jk} A_{ki}, \end{aligned} \quad (16)$$

503 denoted as retarded and advanced cluster coefficients.

504 Given a stationary system, time reversibility means that the joint prob-
 505 ability of a sequence of numbers is the same as the joint probability of the

506 reversed version of this sequence (Lawrance, 1991). The probability distribu-
 507 tions of the retarded and advanced degrees $\rho(k_i^r)$ and $\rho(k_i^a)$ would then not
 508 deviate much (same for \mathcal{C}_i^r and \mathcal{C}_i^a ; Fig. 11). To test this, the distributions
 509 can be compared by a Kolmogorov-Smirnov (KS) test. This test statistic
 510 provides p -values $p(k)$ and $p(\mathcal{C})$ to assess whether the null-hypothesis of re-
 511 versibility can be rejected (Donges et al., 2013).

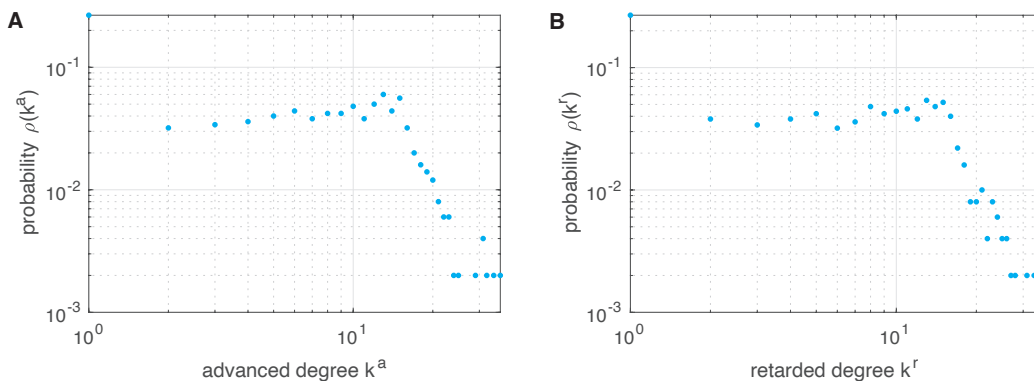


Figure 11: Probability distributions of (A) advanced and (B) retarded degrees $\rho(k_i^a)$ and $\rho(k_i^r)$ of the visibility graph computed from the insolation time series as shown in Fig. 10. The KS-test reveals no significant difference between $\rho(k_i^a)$ and $\rho(k_i^r)$ by a p -value of 1.0, thus, the null hypothesis that the time series is reversible cannot be rejected.

512 This approach has been used to identify a nonlinear regime shift in the
 513 North Atlantic ocean circulation at the onset of the Little Ice Age (Schleuss-
 514 ner et al., 2015), indicating a multi-stability in the Atlantic ocean circulation.
 515 Visibility graphs, in general, are useful tools for several classification and di-
 516 agnostic purposes (Ahmadlou et al., 2010; Zou et al., 2014; Gao et al., 2016;
 517 Supriya et al., 2016).

518 *Software.* The *pyunicorn* package for Python provides tools for studying vis-
 519 ibility graphs (and complex networks in general) (Donges et al., 2015b).

520 3. Data

521 Marine sediments provide insights into geological processes and are widely
 522 used to study the climatological and environmental conditions of the past
 523 (Westerhold et al., 2020). Here we consider marine records of different types
 524 of proxies for the long-term aridification (based on terrigenous dust flux) of
 525 the northern part of the African continent during the Plio-Pleistocene (Trauth

Type	Method	Focus	References
Stochastic modeling	potential analysis	multi stability of underlying processes	Kwasniok and Lohmann (2009); Livina et al. (2010); Kwasniok and Lohmann (2012)
Statistical mechanics and information theory	entropies, order patterns	Time series complexity	Bandt and Pompe (2002); Balasis et al. (2013); Zanin and Olivares (2021)
Phase-space based approaches	recurrence plots, recurrence networks	time series classification, dynamical transitions	Marwan et al. (2007); Boers et al. (2021); Zou et al. (2019)
Visibility relationships	time-directed visibility graphs	temporal reversibility	Lacasa et al. (2012); Donges et al. (2013)

Table 1: Overview on the methods of nonlinear time series analysis discussed and partly compared for applications to Plio-Pleistocene palaeoclimate variability in this study.

526 et al., 2009; Donges et al., 2011a) and the variations in regional temperature
527 and global ice volume (alkenone based SST and benthic $\delta^{18}\text{O}$). Corresponding
528 time series are derived from five sediment records (from West to East;
529 Tab. 2, Figs. 12 and 13):

- 530 • ODP 662 (Atlantic Ocean west of equatorial Africa),
- 531 • ODP 659 (Atlantic Ocean offshore subtropical West Africa),
- 532 • Medisect (Mediterranean on the south coast of Sicily and Calabria),
- 533 • ODP 967 (Eastern Mediterranean Sea),
- 534 • ODP 721/722 (Arabian Sea).

535 They have a sufficient temporal resolution of an average sampling time rang-
536 ing from 0.4 ka up to 4.3 ka. A high temporal resolution is necessary for
537 performing time series analysis (in particular for time-resolved/ windowed
538 analysis).

539 4. Results

540 We apply nonlinear time series analysis as described in Sect. 2 to the
541 marine Plio-Pleistocene proxy records in order to investigate and characterise
542 the dynamics of transitions between the wet and arid climate in the Northern
543 part of Africa (considering the time scale given by the sampling, i.e., we
544 discuss dynamical variations at time scales of $> 1,000$ years). Before we

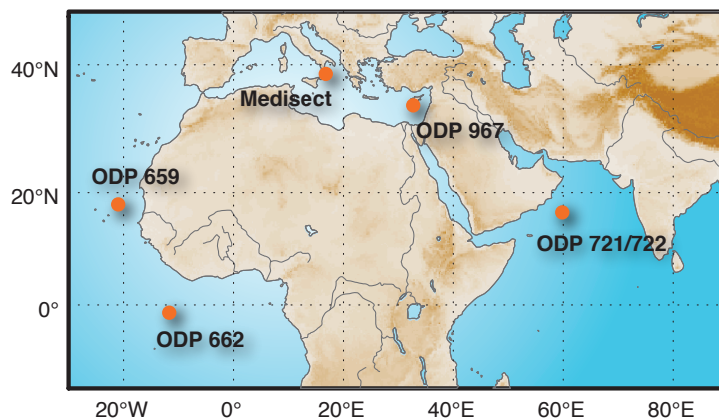


Figure 12: Map of North Africa and surrounding ocean basins with indications of the archives used in this work.

545 compare all proxy records, we will focus on one record (terrigenous dust flux
 546 proxy from ODP659) and explain our findings in more detail. The used
 547 parameters for the methods are provided in Tab. 3.

548 *4.1. Results for dust flux proxy from ODP659*

549 The studied measures of nonlinear time series analysis reveal different
 550 aspects regarding the dynamical properties. The measures are calculated
 551 within overlapping windows of length 410 ka (41 ka offset) to investigate
 552 changes in the dynamics (e.g., to identify regime transitions between more
 553 periods and more erratic climate variability). This implies that a single point
 554 in the resulting time series of measures corresponds to a period of 410 ka,
 555 two consecutive points correspond to 410+41 ka, and so on.

556 In the considered period, several known climate regime transitions occurred.
 557 The most prominent change is the transition from the Pliocene to
 558 the Pleistocene, around 2.6 Ma ago, with the onset of cyclical glaciations in
 559 the northern hemisphere (onset of northern hemisphere glaciation, NHG).
 560 During the Pliocene, a significant tropical climate reorganization with the
 561 development of a strong Walker circulation (intensified Walker circulation,
 562 IWC) occurred between 4.5 and 4.0 Ma (Ravelo et al., 2004), and the marine
 563 isotope stage M2 with decreased global temperature occurred at 3.3 Ma
 564 (Lisiecki and Raymo, 2005). During the Pleistocene, the mid-Pleistocene
 565 transition (MPT) between 1.1 to 0.7 Ma is important, changing the glacial
 566 cycles from approximately 41 ka to a 100 ka dominant periodicity (Clark
 567 et al., 2006). In the course of the early Pleistocene between 2.2 and 1.5 Ma,

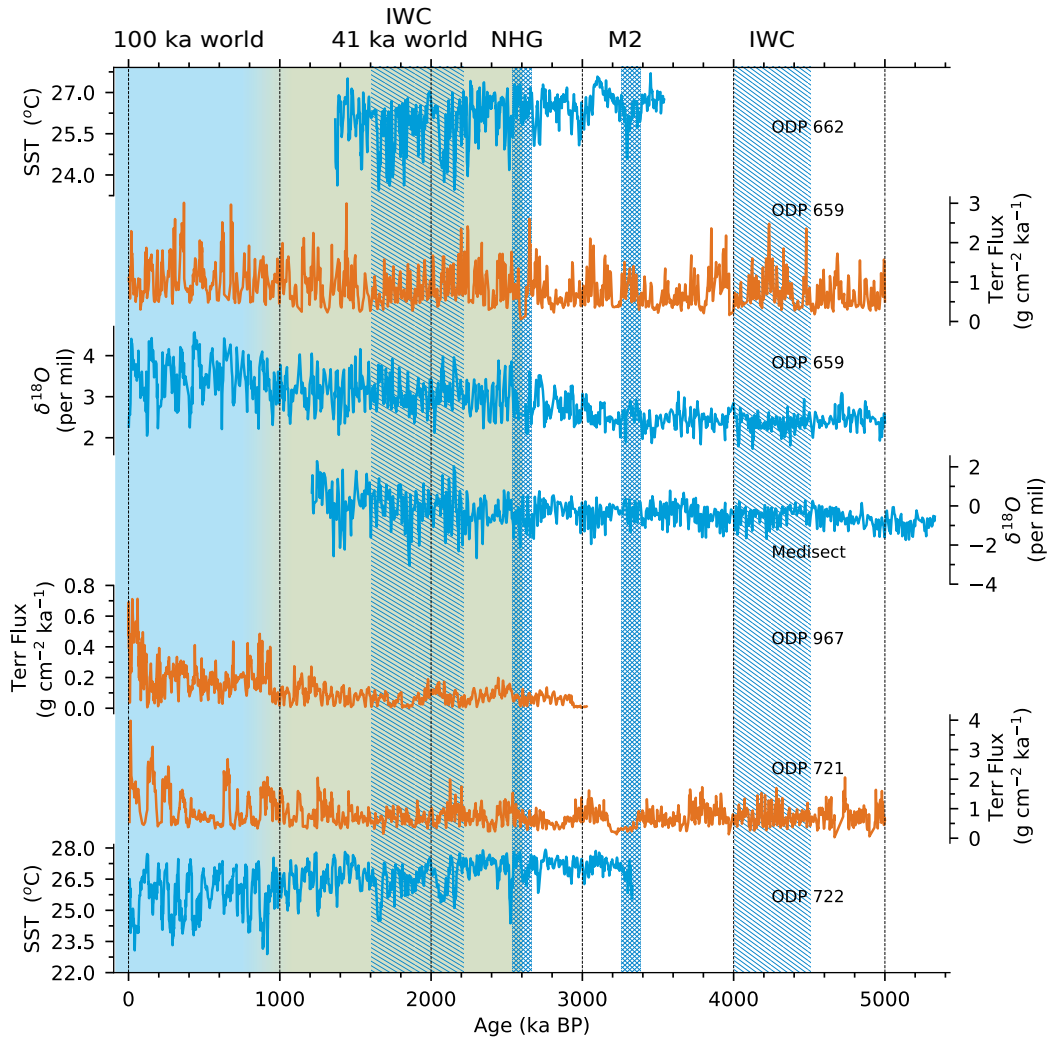


Figure 13: Palaeoclimate time series used in this study (blue – temperature related proxies, orange – terrigenous dust flux proxies) and important climate regimes: IWC – intensified Walker circulation, marine isotope stage M2 with decreased global temperature, NHG – onset of northern hemisphere glaciation (transition from Pliocene to Pleistocene), 41 ka (green shaded) and 100 ka (blue shaded) dominated glacial cycles.

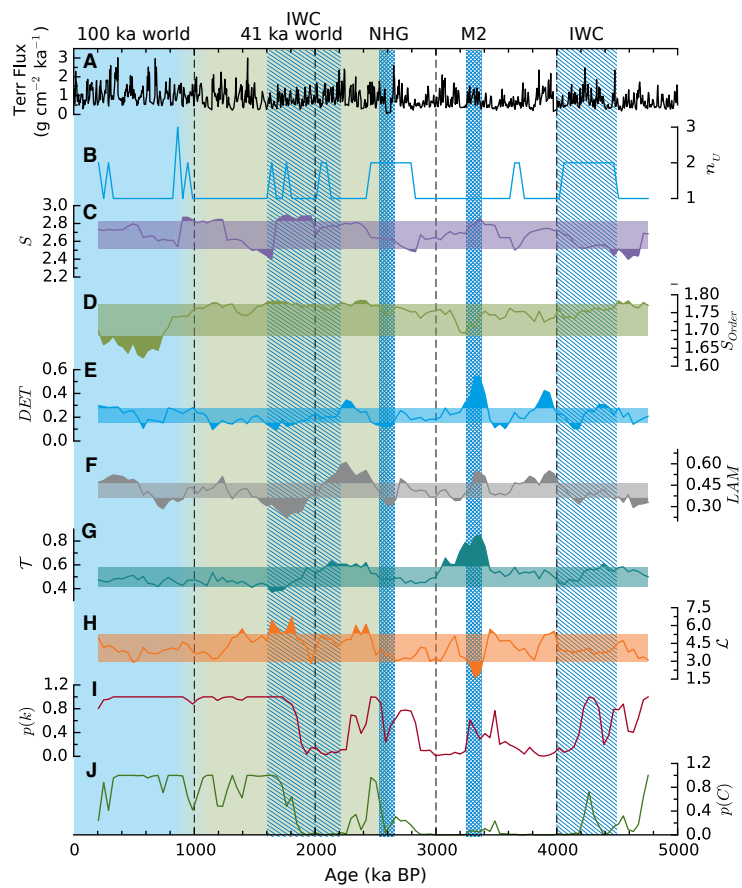


Figure 14: Results for exemplary dust flux proxy record from ODP659 with the important climate regimes as in Fig. 13.

Record	N	Time span (Ma BP)	$\langle\Delta T\rangle$ (ka)	$\sigma(\Delta T)$ (ka)	W	Reference
ODP 662 SST	912	3.54–1.366	2.39	1.05	171	(Herbert et al., 2010)
ODP 659 dust flux	1221	5.0–0.002	4.10	2.69	100	(Tiedemann et al., 1994)
ODP 659 $\delta^{18}\text{O}$	1170	5.0–0.002	4.28	2.88	95	(Tiedemann et al., 1994)
Medisect $\delta^{18}\text{O}$	811	5.33–1.212	5.08	2.06	80	(Lourens et al., 1996)
ODP 967 dust flux	8417	3.028–0.0	0.36	0.31	1139	(Larrasoana et al., 2003)
ODP 721 dust flux	2757	5.0–0.006	1.81	1.52	226	(deMenocal, 1995; DeMenocal, 2004)
ODP 722 SST	1680	3.33–0.007	1.98	0.89	207	(deMenocal, 1995; DeMenocal, 2004)

Table 2: Basic properties of the analysed palaeoclimate time series. N is the number of samples contained in the time series, $\langle\Delta T\rangle$ the mean sampling interval, and $\sigma(\Delta T)$ the standard deviation of sampling intervals (to illustrate the spread of the sampling intervals). The desired window size is $W^* = 410$ ka. W is the corresponding average number of sampling points covering this time span.

Methods	Parameters
Shannon entropy	number of bins $N_{\text{bins}} = 20$
Order entropy	dimension $d = 3$, lag $\tau = 1$
Potential analysis	standard deviation stochastic process $\sigma = 1.5$
Recurrence analysis	fixed recurrence rate $RR = 0.05$, embedding dimension $m = 3$, embedding delay $\tau = 2$, $l_{\text{min}} = 2$, $v_{\text{min}} = 2$
Visibility graph	horizontal visibility
Windowing	window size $w = 410$ ka window step $ws = 41$ ka
Confidence interval	number of surrogates $N_{\text{surr}} = 5,000$ 5% and 95%-quantiles

Table 3: Parameters used for the selected methods in this study (τ , l_{min} , and v_{min} are in sampling time).

568 another significant tropical climate reorganization with intensification and
569 spatial shift of the Walker circulation (IWC) occurred (Ravelo et al., 2004).

570 Potential analysis detects the number of potential wells from the time
571 series, interpreted as the number of (stable) climate states. Singular excursions
572 are neglected because the specific regimes should be identified over at
573 least two consecutive windows to ensure the robustness of our results. The
574 number of climate states n_U changes between one and two (Fig. 14B). For
575 most of the time, there is only one stable climate state, according to poten-
576 tial analysis. Starting at 4.6 Ma, corresponding to the time of known large
577 scale tropical atmospheric reorganization, the African climate bifurcates to a
578 two-state climate, lasting for approx. 800 ka (taking the window length into
579 account), indicating that the climate system was alternating between two

580 major climate states. A similar epoch can be found at the transition from
581 the Pliocene to the Pleistocene between 2.8 Ma and 2.4 Ma and the MPT
582 between 1.0 and 0.8 Ma. Further epochs with indicated double-well potential
583 are too short-lived to be considered as reliable.

584 Next, the two entropy measures are calculated. The windowed Shannon
585 entropy of the time series identifies changes in the amplitude distribution
586 of the proxy values. In contrast, the order entropy considers the dynamics
587 and, thus, identifies changes in the dynamics instead of the proxy's value
588 distribution. The values of the Shannon entropy vary slightly between 2.4
589 and 2.9 (Fig. 14C). In order to interpret the variation as tending to larger or
590 smaller values, we apply a significance test based on a bootstrap-based con-
591 fidence interval. Only entropy values outside the confidence interval will be
592 interpreted as a significant increase or decrease. Significant smaller values in-
593 dicating an unusually peaked amplitude distribution occur during the epoch
594 between 4.8 and 4.5 Ma (before the tropical atmospheric reorganisation) and
595 around 1.6 Ma (after the IWC); increased values, indicating a broader (less
596 peaked) amplitude distribution, occur between 2.0 and 1.6 Ma and around
597 1.0 Ma, corresponding to IWC and the MPT, respectively. However, the
598 values exceed the significance interval only slightly. The order entropy varies
599 within the confidence interval up to the MPT at 0.8 Ma, after which it de-
600 creases significantly to lower values (Fig. 14D). Before this point of time,
601 it only slightly increases indicating more complex dynamics during 4.8 and
602 4.6 Ma (before the tropical atmospheric reorganisation), around 2.4 Ma (at
603 the onset of northern hemisphere glaciation), and during the tropical atmo-
604 spheric reorganisation between 1.8 and 1.6 Ma. At the MPT 800 ka ago, the
605 dynamics changed to significantly less complex dynamics.

606 In the following, we consider the measures related to recurrence analysis.
607 The measure determinism (DET) significantly changes over time (Fig. 14E).
608 A significant increase occurs between 4 and 3.8 Ma (after the period of
609 stronger Walker circulation), between 3.4 and 3.2 Ma (during M2), and
610 around 2.2 Ma (just after the onset of northern hemisphere glaciation). Less
611 pronounced decreases occurred around 4.2 Ma (before the period of stronger
612 Walker circulation), 3.5 Ma (before M2), 2.5 Ma (at the onset of glaciation),
613 and between 1.8 to 1.6 Ma (during the IWC). The increased determinism val-
614 ues indicate intervals of more predictable (e.g., periodic) variability, whereas
615 low values indicate a more random variation. Laminarity (LAM) shows sig-
616 nificant increases similar as DET (Fig. 14F) after the period of stronger
617 Walker circulation (between 4 and 3.8 Ma), during M2 (between 3.4 and

618 3.2 Ma), and during the onset of the glaciation (between 2.5 and 2 Ma).
619 Additionally, after the MPT (after 500 ka), LAM again increases. Increased
620 LAM can be an indication for more persistent dynamics. In contrast, signif-
621 icantly lower LAM values can be found before the period of stronger Walker
622 circulation between 5 and 4.6 Ma, but also during the stronger Walker cir-
623 culation between 2 and 1.6 Ma. At the MPT (between 1.0 and 0.6 Ma) the
624 LAM is also lower than usual.

625 The (recurrence) network based measure transitivity \mathcal{T} displays a similar
626 behaviour as DET, with increased values during the M2 between 3.5 and
627 3.0 Ma and after the onset of the glaciation between 2.5 and 2.2 Ma; as well
628 as a decrease during the period of IWC at around 1.8 Ma. Although this
629 measure represents different nonlinear aspects of the dynamics, it can also be
630 interpreted in the sense of more regular (larger values) or more random (low
631 values) variability. The different regimes indicated by both measures during
632 the same time intervals support the hypothesis of climatological changes
633 between more variable and more regular climate variability. The average
634 path length highlights the timing of the onsets of abrupt regime changes.
635 This measure indicates abrupt changes at M2 (3.3 Ma), at the transition
636 from the Pliocene to the Pleistocene (onset of NHG) and the Pleistocene
637 IWC.

638 Finally, the temporally directed topological properties of the visibility
639 graphs are used to test whether the considered periods behave like a nonlin-
640 ear process (by testing for reversibility). This is performed by considering
641 the p -values of the KS-test (Subsect. 2.5). Very small p -values indicate peri-
642 ods of time irreversibility or non-stationarity, suggesting nonlinear behaviour
643 during these times. Both measures, based on degree and clustering coeffi-
644 cient, behave very similarly. Only during the time intervals after the IWC
645 (after 4.0 Ma) and up to the M2 (3.3 Ma), between the M2 and the transition
646 phase to the Pleistocene (3.2 to 2.8 Ma), as well as during the time after the
647 IWC (between 2.2 and 1.8 Ma), the time reversibility had to be rejected,
648 suggesting more nonlinear behaviour. Overall, a pattern emerges indicat-
649 ing more nonlinear climate dynamics (more complex) before approx. 2.0 Ma
650 during the Pliocene and early Pleistocene, and more linear variability (less
651 complex) during the Mid- and late Pleistocene.

652 4.2. *Unified view on North African Plio-Pleistocene climate*

653 In the following, we will investigate and discuss the dynamics of the dust
654 flux and SST proxy records using the selected measures order entropy (S_{order}),

655 number of states (n_U), determinism (DET), and time reversibility ($p(\mathcal{C})$).
 656 The proxy time series reflect conditions of regional temperature (provided by
 657 Alkenone based SST estimations and $\delta^{18}\text{O}$) and African aridity (terrigenous
 658 dust flux) at different locations.

659 *Order entropy.* The order entropy of the tropical SST records reveals an in-
 660 crease in the complexity of the temperature dynamics in the subtropics dur-
 661 ing the IWC (Fig. 15A, G). The $\delta^{18}\text{O}$ temperature proxy from the ODP659
 662 site presents a similar increase in complexity during the Pliocene IWC, but
 663 not during the Pleistocene IWC (Fig. 15C). At the Medisect region, S_{order}
 664 does not show any (significant) influence of the IWC on the climate dynamics
 665 (Fig. 15D).

666 The dynamical complexity of the dust flux records shows regional dif-
 667 ferences. During the Pliocene IWC, the complexity is slightly increased in

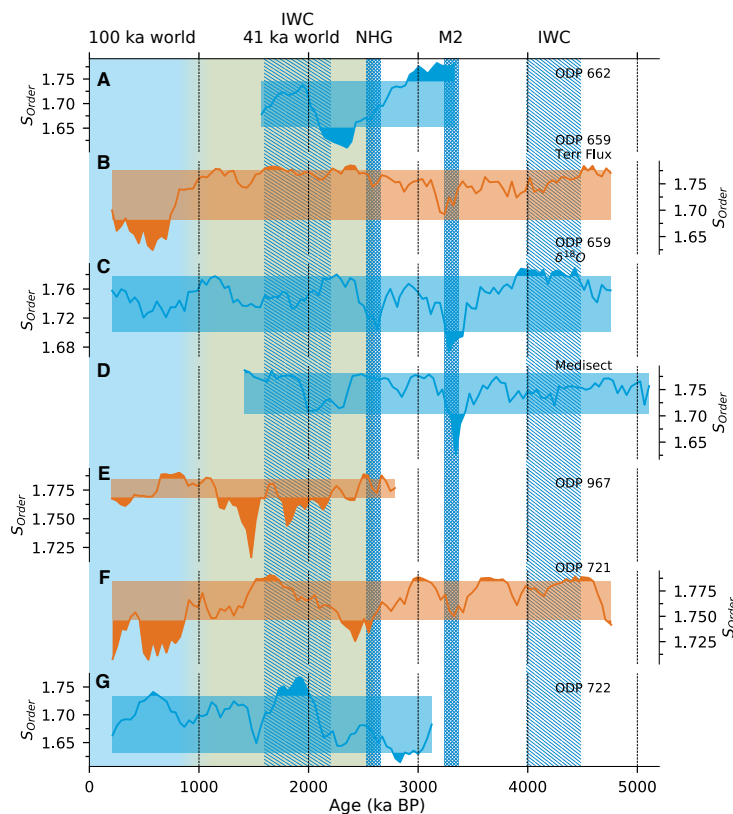


Figure 15: Order entropy (or permutation entropy) of the analysed palaeoclimate proxy series.

668 the Arabian sea (Fig. 15F), while it is less affected in the subtropical At-
669 lantic (Fig. 15B). During the Pleistocene IWC, the dynamical complexity is
670 only slightly increased at the end of the corresponding time interval, when
671 the large-scale atmospheric circulation pattern is changing to less intensive
672 Walker circulation. In contrast, in the eastern Mediterranean, the complexity
673 is even significantly reduced (Fig. 15E).

674 During the M2 cooling event, the complexity in the dynamics in all proxies
675 and sites covering this event is reduced (Fig. 15B, C, D, F).

676 The onset of northern hemisphere glaciation is related to a short and slight
677 increase in the dynamical complexity of the dust flux in the tropical Atlantic
678 and in the eastern Mediterranean (Fig. 15B, E), but a decrease of complexity
679 in the Arabian sea (Fig. 15F). This reduced complexity due to the glacial
680 cycles is also visible in the SST proxy of the tropical Atlantic (Fig. 15A),
681 but not in the northern subtropical Atlantic or the Arabian sea (Fig. 15C,
682 G). This is a sign for a reorganisation of the atmospheric circulation pattern
683 due to the beginning of the glaciation, a pattern that is later changed again
684 during the Pleistocene IWC.

685 The transition from the 41 ka to the 100 ka dominated glaciation cycles
686 after the MPT is related to a reduction of the dynamical complexity in the
687 dust flux records (Fig. 15B, E, F). In the eastern Mediterranean, this happens
688 later than in the Arabian sea.

689 *Potential analysis.* The potential analysis reveals an increase in the number
690 of states during the IWC (Fig. 16). Here we can find slight differences be-
691 tween the regions and proxies. During the Pliocene, this increase is most
692 clearly visible in the west, in the dust flux record, and less clear in the east,
693 but opposite during the Pleistocene (Fig. 16B, E, F).

694 The potential analysis of the SST proxy in the Arabian sea shows different
695 results than for the other SST proxies. It suggests more states after the onset
696 of glaciation, but a reduced number of states during the IWC (Fig. 16A, D,
697 G), which can be a sign of a different ocean circulation regime in the Indian
698 Ocean during this time.

699 *Recurrence analysis.* The recurrence plot based determinism measure shows
700 clear differences in the absolute values of the SST proxies (< 0.5) and the
701 terrigenous dust flux records in the Arabian sea and the eastern Mediter-
702 ranean, with values up to 0.98 in the ODP967 record. The ODP967 record
703 should be considered a bit different here, because larger temporal resolution

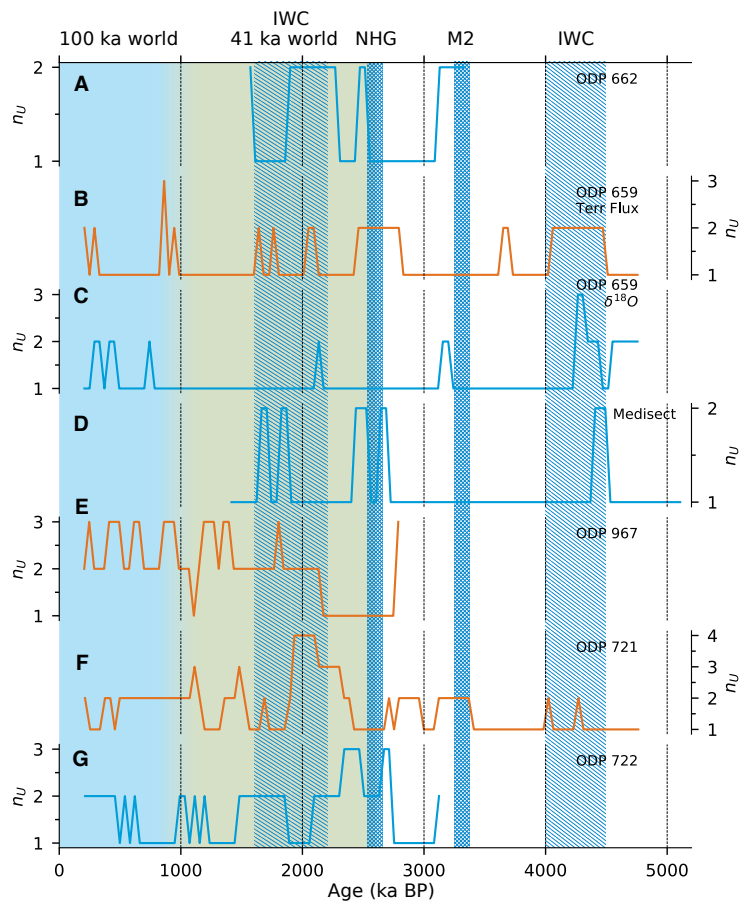


Figure 16: Potential analysis of the analysed palaeoclimate proxy series.

704 (as it is the case in ODP967) is causing more longer lines in recurrence plots
 705 and shifts DET towards larger values. Therefore, by using the significance
 706 test we discuss the variation in DET in a relative way.

707 We find an increase to more predictable dynamics (as typical for periodic
 708 or cyclic dynamics) after the onset of the cyclical NHG in the terrigenous
 709 dust flux records in the eastern Mediterranean and the subtropical Atlantic
 710 (Fig. 17B, E), but also in the SST dynamics of the Medisect site, and slight
 711 or tending increase (although partly not significant) in the tropical Atlantic
 712 and the Arabian sea (Fig. 17A, D, G).

713 The M2 event is also characterised by more predictable variability of the
 714 dust flux records (Fig. 17B, F), but does not affect the dynamics of the
 715 temperature dynamics in general (Fig. 17A, D), except for the subtropical

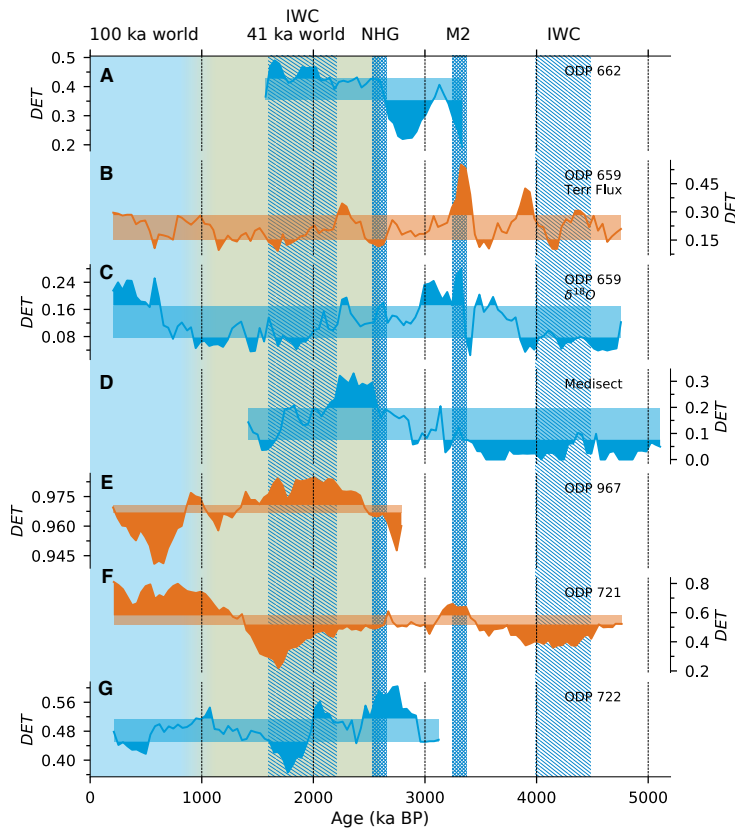


Figure 17: Determinism measure of the analysed palaeoclimate proxy series.

716 Atlantic (those DET values are in general quite low, Fig. 17C).

717 During the Pleistocene IWC, the dust flux in the eastern Mediterranean
 718 shows a remarkable increase in the DET values (Fig. 17E), confirming the
 719 finding based on order entropy that the dynamics becomes more regular and
 720 predictable.

721 After the MPT, the dynamics becomes remarkably more predictable in
 722 the Arabian sea, but less predicable in the eastern Mediterranean (Fig. 17E,
 723 F). Interestingly, the site ODP659 does not show significant change in this
 724 respect, although the order entropy has shown a decrease of dynamical com-
 725 plexity in this region, too (Figs. 17B and 15B).

726 *Time reversibility (nonlinearity) test.* The test for time reversibility as an
 727 indicator of nonlinearity (based on $p(\mathcal{C})$) of the proxy records shows regional
 728 differences. In the tropical west, a nonlinear behaviour in the temperature

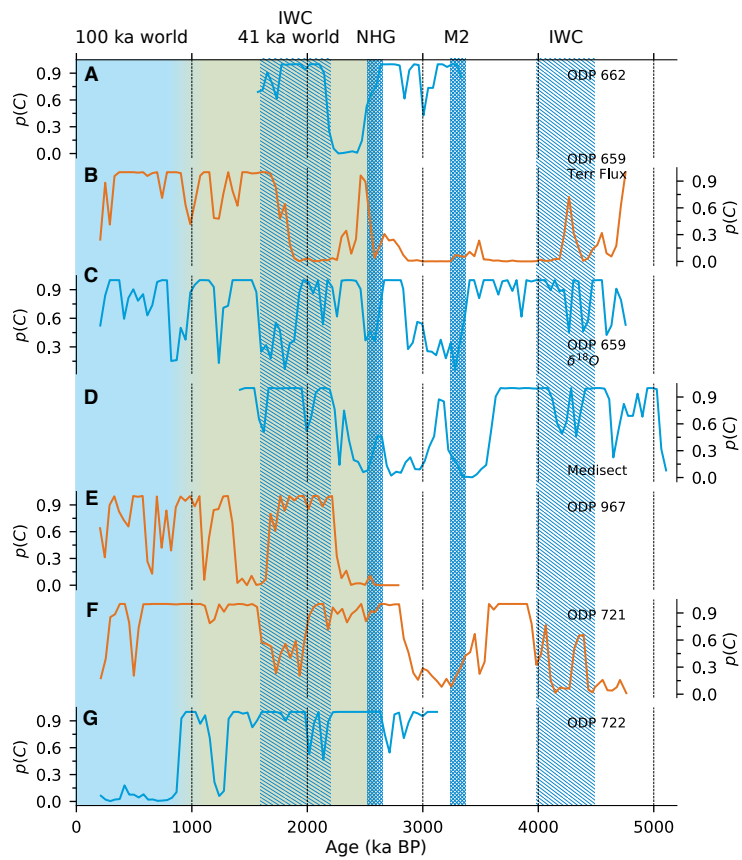


Figure 18: Time series irreversibility indicator based on p -values of the visibility graph clustering coefficients for the analysed palaeoclimate proxy series (only very small p -values indicate significance).

729 (SST) dynamics is only indicated after NHG onset and lasting until the
730 Pleistocene IWC (Fig. 18A). In the subtropical west, there is almost no
731 significant p -value for the SST nonlinearity, except for very short times at
732 the M2 event and in the second half of the Pleistocene IWC (Fig. 18C). In the
733 Mediterranean region, nonlinear dynamics is indicated before and during the
734 M2 event, as well as before the onset of the NHG (Fig. 18D). In the Arabian
735 sea, we only find nonlinear behaviour for the SST dynamics just before and
736 after the MPT (Fig. 18G).

737 The analysis of the terrigenous dust flux records indicates short periods
738 of nonlinear behaviour before and during the Pliocene IWC and during the
739 Pleistocene IWC (Fig. 18B, F), whereas the East Arabian site responds later
740 than the western site. In contrast, we do not find such a nonlinear dynamics
741 in the eastern Mediterranean during the Pleistocene IWC (Fig. 18E), but
742 before and after this IWC. After the M2 cooling event, nonlinear behaviour
743 in the dust flux records is found in the East Arabian sea and the subtropical
744 Atlantic.

745 5. Discussion

746 The considered methods of nonlinear time series analysis reveal different
747 aspects of Africa's aridification and regional temperature variations during
748 the Plio-Pleistocene. When directly comparing the corresponding measures,
749 we find that they are not or only slightly correlated to each other (Fig. 19),
750 but allow us to interpret them from a dynamical point of view by providing
751 complementary information, as we discuss in more detail below for several
752 key climate events in this epoch (as mentioned above, the dynamical variation
753 discussed here occurs at time scales $> 1,000$ years).

754 *Intensified Walker circulation (IWC)*. The IWC appears to be generally re-
755 lated to a dynamics with a larger number of possible quasi-stable states, in
756 Africa's aridity (represented by the proxy records at ODP659 and ODP721)
757 as well as in the regional temperature (indicated by n_U). The transition to
758 this regime during the Pliocene is characterised by a significant change in the
759 amplitude distributions of the dust flux data from less to more complex am-
760 plitude distributions (indicated by elevated S for ODP659), corresponding
761 to the increased number of states. Similarly, during the Pleistocene, we find
762 a transition from high to low complexity amplitude distribution when this
763 specific regime terminated. During the onset of the Pliocene IWC period, we

764 find slight but significant increases of the complexity in the dynamics during
765 the transition phase in African hydro-climate as represented by ODP659 and
766 ODP721 (indicated by increased S_{order}). Similar to the change in the ampli-
767 tude distributions at the termination of the Pleistocene IWC, we find a drop
768 in the complexity of the dynamics at this transition. The IWC also comes
769 along with a shift from more regular, predictable, and persistent dynam-
770 ics to less regular, less predictable, and less persistent dynamics (\mathcal{T} , DET,
771 LAM). Moreover, the Pleistocene IWC seems to behave rather nonlinear,
772 whereas during the Pliocene IWC this cannot be clearly identified, although
773 a tendency is visible (indicated by low $p(k)$ and $p(\mathcal{C})$ values). Overall, these
774 results suggest that the IWC is related to a 2-state regime in African cli-
775 mate (e.g., alternating between wetter and drier conditions), confirmed by
776 the more complex amplitude distribution and the nonlinear behaviour, as
777 well as with a less predictable and less persistent dynamics.

778 The terrigenous dust flux record at ODP site 967 (eastern Mediter-
779 ranean) covers only the Pleistocene IWC and differs from the above obser-
780 vations. In contrast to the subtropical Atlantic and Arabian sea site, the
781 eastern Mediterranean shows a remarkable increase in regularity and pre-
782 dictability during the IWC (low S_{order} and large DET), suggesting a change
783 in the tropical rainbelt.

784 Based on the $\delta^{18}\text{O}$ and SST proxies, we also find clear spatial differences
785 in the temperature dynamics in the Atlantic, Mediterranean, and Arabian
786 sea regions. With beginning IWC, in the (sub-)tropical Atlantic the number
787 of states is increasing whereas it is decreasing in the Arabian sea. At the
788 same time, temperature dynamics becomes less predictable and less regular
789 during the Pleistocene IWC in all regions.

790 *Marine isotope stage M2.* The marine isotope stage M2 is a relatively short
791 period of colder global climate. It is related to more predictable and per-
792 sistent dynamics in Africa's hydro-climate (low S_{order} and large DET, LAM,
793 and \mathcal{T}). The subtropical Atlantic and Mediterranean temperature variability
794 is also becoming less complex and more predictable (low S_{order} , increase in
795 DET to intermediate and larger values).

796 In contrast, the tropical Atlantic shows a more complex and much less
797 predictable dynamics during the M2 event (high S_{order} and low DET).

798 Following M2, the dynamics of African hydro-climate becomes again less
799 predictable (average values of DET, LAM, and \mathcal{T}) and more nonlinear (in-
800 dicated by $p(k)$ and $p(\mathcal{C})$).

801 These results could be interpreted in the sense that the cooling event has
802 caused some cyclical variation between cold and warm temperatures in the
803 northern hemisphere (anticipating the glacial oscillations at high latitudes
804 during the late Pleistocene) and wet and dry climate in Africa, whereas
805 in the tropics, no such cyclical changes occurred. However, the differences
806 between these were not strong enough to cause a bifurcation of the system
807 with two clearly different emerging states.

808 *Onset of northern hemisphere glaciation.* During the transition from Pliocene
809 to Pleistocene, African hydro-climate dynamics clearly shifts to a less pre-
810 dictable and less persistent regime (low DET values). This appears to be
811 related to a short-lived shift to more regular and less complex dynamics in
812 the Arabian sea. After this transition phase, the dynamics becomes clearly
813 more predictable and persistent in African hydro-climate, the tropical At-
814 lantic, the Mediterranean region, and the Arabian sea, mainly as a result of
815 the onset of cyclical glaciations.

816 *Mid-Pleistocene transition (MPT).* The MPT is characterised by a change
817 from more to less complex amplitude distributions (indicated by S in the
818 ODP659 dust record), and by a decrease in dynamical complexity (indicated
819 by significant drop in S_{order}). Around the time of the transition, the co-
820 occurrence of 41 ka and 100 ka cycles (Trauth et al., 2009) causes an increase
821 in the number of possible system states (increase in n_U to 2 and even 3 in
822 the dust flux proxies) and a less persistent dynamics (decreased LAM). After
823 500 ka, the dynamics becomes more and more predictable and persistent as
824 the 100 ka cycles become more and more dominant (increasing DET val-
825 ues, decreasing S_{order} , except for the eastern Mediterranean). Consistently,
826 climate variability is largely time reversible, indicating dominance of rather
827 linear dynamics (large values of $p(k)$ and $p(\mathcal{C})$), with the remarkable excep-
828 tion of the Arabian sea, which shows a more nonlinear behaviour during the
829 100 ka world.

830 The MPT has not only changed the dynamics from a dominance of 41 ka
831 to 100 ka cyclicity, but also caused a regime change in the Arabian sea towards
832 more nonlinear dynamics by additional influences, e.g., by cooling-warming
833 cycles and changes in the meridional overturning circulation in the Indian
834 ocean, or increased Indonesian throughflow after the MPT (Petrick et al.,
835 2019).

836

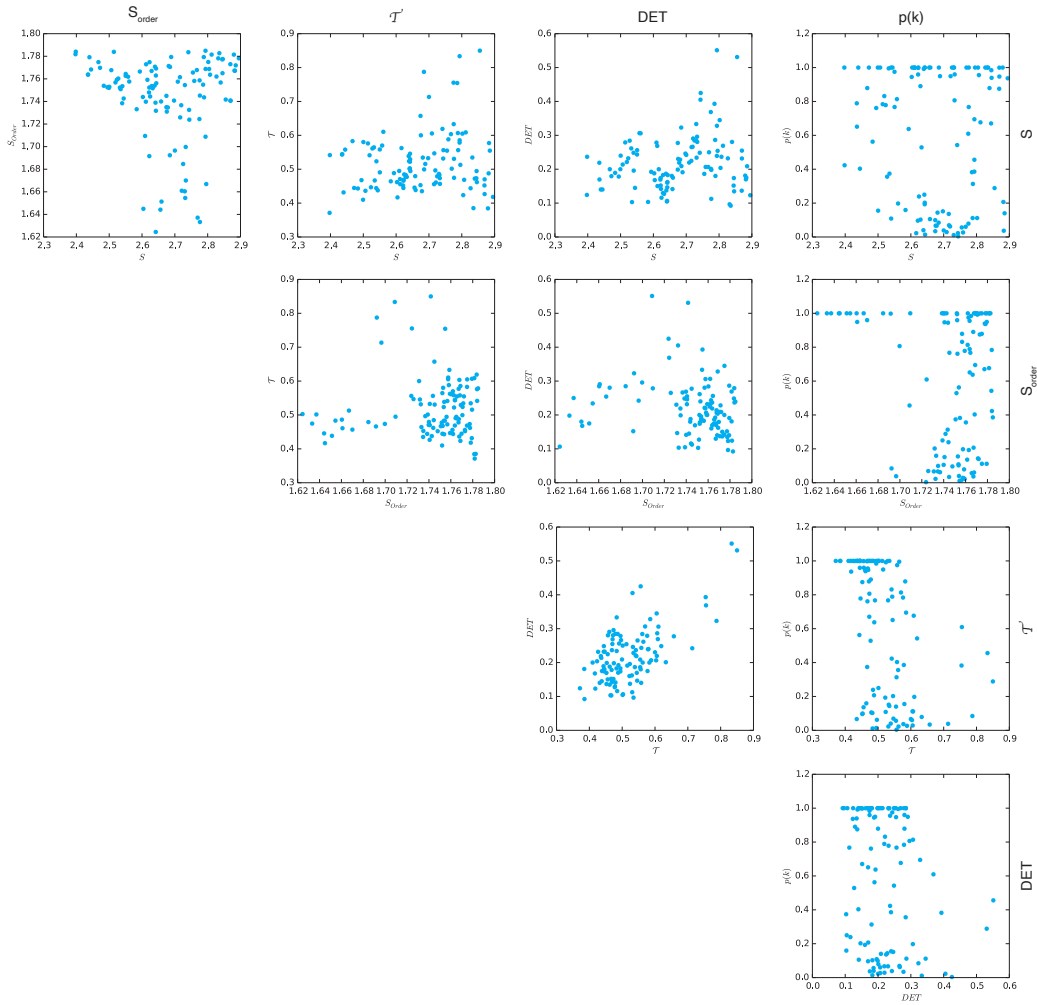


Figure 19: Comparison of selected measures of nonlinear time series analysis for the ter-rigenous dust flux record ODP659 (scatter plots).

837 The nonlinear analysis applied here covers different aspects, such as prop-
 838 erties of the proxies' windowed amplitude distributions, complexity and pre-
 839 dictability of the dynamics, nonlinear vs. linear dynamics, or multi-stability.
 840 As described above, such properties can change on longer time scales. One of
 841 the most important drivers of those climate regime changes are orbital vari-
 842 ations in insolation in the form of Milankovich cycles, as is already obvious
 843 from the indicated dynamical changes when northern hemisphere glaciation
 844 sets in or when glacial cycles change from 41 to 100 ka dominant periodicity.
 845 This relationship is not directly visible in the proxy data, e.g., when applying
 846 linear methods, such as correlation and regression analysis (Fig. 20).

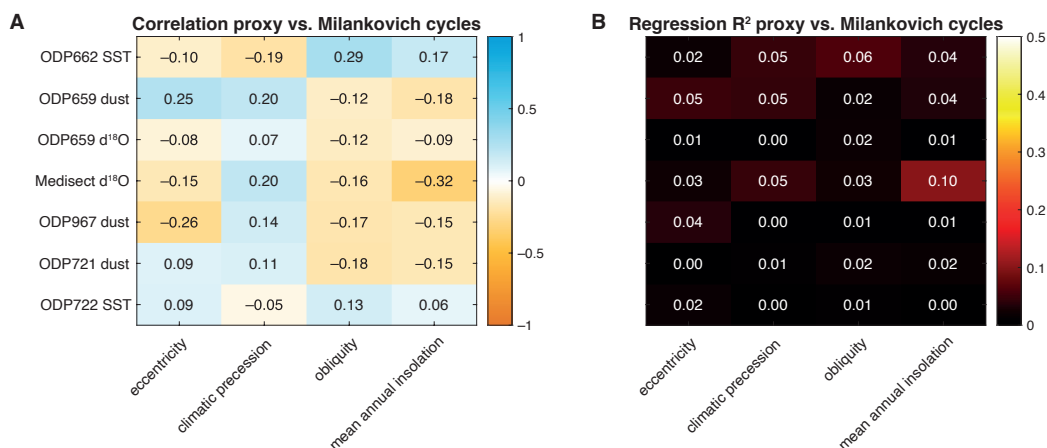


Figure 20: (A) Pearson correlation and (B) coefficient of determination (R^2) between the original proxy data and the Milankovich cycles (interpolated to the time axis of the corresponding proxy), indicating no pronounced linear relationship between proxies and Milankovich cycles.

847 In contrast, several measures of nonlinear time series analysis are more
 848 clearly related to the Milankovich cycles (Figs. 14 to 18). Comparing the
 849 individual components of the Milankovich cycles, we find that the variation
 850 of obliquity is significantly correlated to several regime shift indicators, in
 851 particular for the proxies from ODP662 and ODP967 (Fig. 21). A larger
 852 obliquity causes more pronounced seasonality and its change triggers the on-
 853 set of interstadials and stadials. A closer look at the relationship with obli-
 854 quity reveals differences in the dynamical properties between the Pliocene,
 855 the early Pleistocene before the MPT, and the later Pleistocene after the
 856 MPT (Fig. 22). During the Pleistocene, the dynamics is more regular and

857 predictable (increasing DET), due to the more cyclical variations (glacial
 858 cycles).

859 Moreover, we find spatial differences in the dynamics represented by the
 860 terrigenous dust flux proxies (e.g., Fig. 21A). The site in the eastern Mediter-
 861 ranean behaves mainly opposite to the site in the Atlantic and the Arabian
 862 sea. This result suggests a specific pattern in atmospheric circulation or the
 863 tropical rainbelt the change of which is affecting the subtropical regions east
 864 and west of Africa differently than in the north.

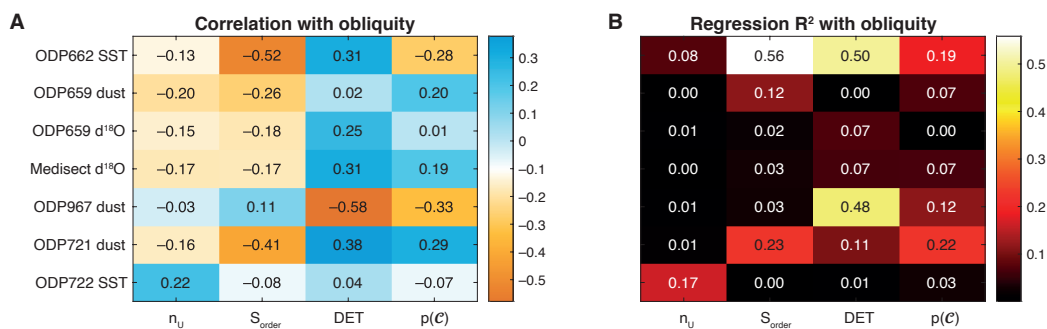


Figure 21: (A) Pearson correlation and (B) coefficient of determination (R^2) between selected quantifiers of nonlinear time series analysis and the obliquity cycles (interpolated to the time axis of the corresponding proxy), indicating significant relationships between some of the dynamical regime changes in temperature and African hydro-climate and the seasonality inducing obliquity variation.

865 While these measures of nonlinear time series analysis reveal interesting
 866 insights in the changing climate dynamics, there are some important method-
 867 ological aspects to be considered (Marwan, 2011). Entropy measures and
 868 potential estimation rely on good estimates of probability density functions
 869 and, thus, require long time series. Recurrence and network based methods
 870 can be applied on shorter time series, but may be biased by missing data
 871 or irregular sampling as it is common in palaeoclimate data. As we have
 872 seen, higher temporal resolution can shift values in certain measures (e.g., in
 873 DET). This is not a problem as long as we compare the variations only within
 874 a single record in a relative manner (as performed in this study). If direct
 875 comparison of absolute values is required, the data needs to be resampled
 876 to a common time axis. New approaches to reduce the biases induced by
 877 irregular sampling and simple interpolation approaches have been suggested,
 878 using time slotting, Gaussian kernel based interpolation, or transformation
 879 cost approaches (Babu and Stoica, 2010; Rehfeld et al., 2011; Ozken et al.,

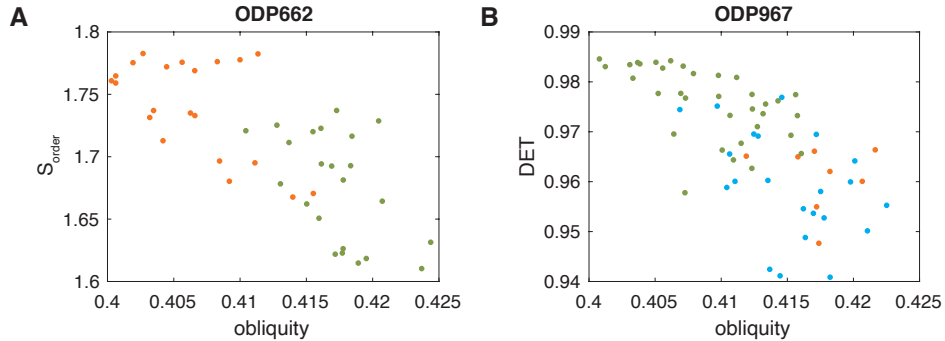


Figure 22: (A) Pearson correlation and (B) coefficient of determination (R^2) between selected quantifiers of nonlinear time series analysis and the obliquity cycles (interpolated to the time axis of the corresponding proxy), indicating a significant relationship between some of the dynamical regime changes in the temperature and African’s hydroclimate and the seasonality inducing obliquity variation. The colour represents the Pliocene (orange), early Pleistocene before the MPT (green) and the late Pleistocene after the MPT (blue).

880 2015; Eroglu et al., 2016). The phase space reconstruction by time delay
 881 embedding as employed in this study can also cause spurious correlations,
 882 leading to an overestimation of deterministic dynamics. Therefore, alterna-
 883 tive embedding concepts could play an increasing role in the future (Lekscha
 884 and Donner, 2018; Kraemer et al., 2021). Further bias can be caused by dat-
 885 ing uncertainties and tuning to a target signal, e.g., astronomical tuning to
 886 the Milankovich cycles. The latter, in particular, is a serious problem when
 887 performing spectral or wavelet analysis (Blaauw, 2012). Although this tuning
 888 can also change the spatial distribution of line structures in recurrence plots,
 889 it is not a problem for recurrence quantification analysis, because it is based
 890 on the distribution of the line lengths, which is not strongly affected by the
 891 tuning. Nevertheless, novel definitions of recurrences, which even incorporate
 892 uncertainties (such as those coming from dating), might receive interest in the
 893 future also for palaeoclimate studies (Goswami et al., 2018). The synthesis
 894 of a large number of palaeoclimate records is not a simple task and can lead
 895 to confusing results. Complex networks can provide the necessary abstrac-
 896 tion level that helps to declutter and highlight relevant spatial and process
 897 relationships (Rehfeld et al., 2013; Boers et al., 2021). For such purposes,
 898 we might also be interested in the interrelationships or directed couplings
 899 between those records. Usually, different sampling resolutions and dating
 900 uncertainties are a major problem which impedes the application of methods

901 such as Pearson correlation, information transfer, synchronisation analysis,
902 or Granger causality. Although new approaches have been suggested in the
903 last years which try to overcome these challenges, the results should be con-
904 sidered with care (Hannisdal, 2011; Rehfeld et al., 2011; Smirnov et al., 2017).
905 Finally, the interpretability of the obtained results may depend crucially on
906 the palaeoclimate archive or proxy under study, related to the observability
907 of the proxy variable presenting a nonlinear transformation of the (usually
908 unknown) climatic driver (Lekscha and Donner, 2020). But this is a gen-
909 eral problem and applies to any statistical analysis of palaeoclimate proxy
910 records.

911 **6. Conclusions**

912 In this review we have considered selected approaches from nonlinear
913 time series analysis and applied them to marine palaeoclimate proxy records
914 of African climate variations during the Plio-Pleistocene. We have shown
915 that these methods reveal different aspects in the dynamics of the palaeo-
916 climate and complement each other. In general, this approach can be used
917 to study palaeoclimate regime changes. We have illustrated this approach
918 by identifying and characterising changes in palaeoclimate during the Plio-
919 Pleistocene, associated to significant events and transitions such as the ma-
920 rine isotope stage M2, the onset of the northern hemisphere glaciation, and
921 the mid-Pleistocene transition. Compared to linear analysis or simple inter-
922 pretations in terms of cooling and stadial-interstadial cycles, nonlinear time
923 series analysis provides deeper insights into the dynamics, such as increasing
924 or decreasing number of climate states (multi-stability), nonlinear vs. linear
925 behaviour, or increasing predictability of the variation due to more cyclical
926 dynamics. The synthesis of the nonlinear time series analysis of different
927 proxy records can be used to make inferences on spatial differences in the
928 impact of global climate drivers such as orbital variations and in changes in
929 large-scale atmospheric patterns.

930 **7. Data and software availability**

931 The data and analysis script used here are available at Zenodo: [doi:10.5281/zenodo.5578298](https://doi.org/10.5281/zenodo.5578298).

Method	Software	Language	URL
Entropy	CRP Toolbox	MATLAB	https://tocsy.pik-potsdam.de/CRPtoolbox/
Order entropy	ordpy	Python	https://github.com/arthurpessa/ordpy
	Permutation entropy	MATLAB	https://mathworks.com/matlabcentral/fileexchange/44161-permutation-entropy-fast-algorithm
Stochastic modelling	scipy	Python	(standard package)
	kramersmoyal	Python	https://github.com/LRydin/KramersMoyal
	Statistics and Machine Learning Toolbox FilterPy	MATLAB Python	(standard package) https://github.com/rlabbe/filterpy
Recurrence plots, recurrence networks	pyunicorn	Python	https://github.com/pik-copan/pyunicorn
	PyRQA	Python	https://pypi.org/project/PyRQA/
	CRP Toolbox	MATLAB	https://tocsy.pik-potsdam.de/CRPtoolbox/
Visibility graphs	pyunicorn	Python	https://github.com/pik-copan/pyunicorn

Table 4: Web addresses of selected software packages providing the methods of nonlinear time series analysis similar to this study.

932 Acknowledgement

933 This study was supported by the DFG projects MA4759/8-1 “Impacts of
934 uncertainties in climate data analyses (IUCliD)”, MA4759/9-1 “Recurrence
935 plot analysis of regime changes in dynamical systems”, MA4759/11-1 “Non-
936 linear empirical mode analysis of complex systems: Development of general
937 approach and application in climate”, by TÜBİTAK (Grant No. 118C236),
938 by the BAGEP Award of the Science Academy, by the Leibniz Association
939 (project DominoES), and the European Research Council (project ERA,
940 ERC-2016-ADG-743080).

941 References

- 942 Afsar, O., Tirnakli, U., Kurths, J., 2016. Entropy-based complexity measures
943 for gait data of patients with Parkinson’s disease. *Chaos: An Interdisci-
944 plinary Journal of Nonlinear Science* 26, 023115. doi:10.1063/1.4942352.
- 945 Ahmadlou, M., Adeli, H., Adeli, A., 2010. New diagnostic EEG markers of

- 946 the Alzheimer's disease using visibility graph. *Journal of Neural Transmis-*
947 *sion* 117, 1099–1109. doi:10.1007/s00702-010-0450-3.
- 948 Albeverio, S., Jentsch, V., Kantz, H. (Eds.), 2006. *Extreme Events in Nature*
949 *and Society*. The Frontiers Collection, Springer Berlin Heidelberg, Berlin,
950 Heidelberg. doi:10.1007/3-540-28611-X.
- 951 Babu, P., Stoica, P., 2010. Spectral analysis of nonuniformly sampled data
952 – a review. *Digital Signal Processing* 20, 359–378. doi:10.1016/j.dsp.
953 2009.06.019.
- 954 Balasis, G., Daglis, I.a., Papadimitriou, C., Kalimeri, M., Anastasiadis,
955 A., Eftaxias, K., 2008. Dynamical complexity in D_{st} time series using
956 non-extensive Tsallis entropy. *Geophysical Research Letters* 35, L14102.
957 doi:10.1029/2008GL034743.
- 958 Balasis, G., Donner, R.V., Potirakis, S.M., Runge, J., Papadimitriou, C.,
959 Daglis, I.A., Eftaxias, K., Kurths, J., 2013. *Statistical Mechanics and*
960 *Information-Theoretic Perspectives on Complexity in the Earth System*.
961 *Entropy* 15, 4844–4888. doi:10.3390/e15114844.
- 962 Bandt, C., Pompe, B., 2002. Permutation entropy - a complexity mea-
963 sure for time series. *Physical Review Letters* 88, 174102. doi:10.1103/
964 PhysRevLett.88.174102.
- 965 Bandt, C., Shiha, F., 2007. Order Patterns in Time Series. *Journal of Time*
966 *Series Analysis* 28, 646–665. doi:10.1111/j.1467-9892.2007.00528.x.
- 967 Barrat, A., Weigt, M., 2000. On the properties of small-world network
968 models. *The European Physical Journal B* 13, 547–560. doi:10.1007/
969 s100510050067.
- 970 Blaauw, M., 2012. Out of tune: The dangers of aligning proxy archives.
971 *Quaternary Science Reviews* 36, 38–49. doi:10.1016/j.quascirev.2010.
972 11.012.
- 973 Boaretto, B.R.R., Budzinski, R.C., Rossi, K.L., Prado, T.L., Lopes, S.R.,
974 Masoller, C., 2021. Evaluating Temporal Correlations in Time Series Us-
975 ing Permutation Entropy, Ordinal Probabilities and Machine Learning.
976 *Entropy* 23, 1025. doi:10.3390/e23081025.

- 977 Boccaletti, S., Latora, V., Moreno, Y., Chavez, M., Hwang, D.U., 2006.
978 Complex networks: structure and dynamics. *Physics Reports* 424, 175–
979 308. doi:10.1016/j.physrep.2005.10.009.
- 980 Boers, N., Kurths, J., Marwan, N., 2021. Complex systems approaches for
981 Earth system data analysis. *Journal of Physics: Complexity* 2, 011001.
982 doi:10.1088/2632-072X/abd8db.
- 983 Boers, N., Rypdal, M., 2021. Critical slowing down suggests that the western
984 Greenland Ice Sheet is close to a tipping point. *Proceedings of the National
985 Academy of Sciences* 118, e2024192118. doi:10.1073/pnas.2024192118.
- 986 Boettner, C., Klinghammer, G., Boers, N., Westerhold, T., Marwan, N.,
987 2021. Early-Warning Signals For Cenozoic Climate Transitions. *Quater-
988 nary Science Reviews* doi:10.1016/j.quascirev.2021.107177.
- 989 Brugger, J., Feulner, G., Petri, S., 2017. Baby, it’s cold outside: Climate
990 model simulations of the effects of the asteroid impact at the end of the
991 Cretaceous. *Geophysical Research Letters* 44, 419–427. doi:10.1002/
992 2016GL072241.
- 993 Burke, K.D., Williams, J.W., Chandler, M.A., Haywood, A.M., Lunt, D.J.,
994 Otto-Bliesner, B.L., 2018. Pliocene and Eocene provide best analogs for
995 near-future climates. *Proceedings of the National Academy of Sciences*
996 115, 13288–13293. doi:10.1073/pnas.1809600115.
- 997 Cao, L., 1997. Practical method for determining the minimum embedding
998 dimension of a scalar time series. *Physica D* 110, 43–50. doi:10.1016/
999 S0167-2789(97)00118-8.
- 1000 Clark, P.U., Archer, D., Pollard, D., Blum, J.D., Rial, J.A., Brovkin,
1001 V., Mix, A.C., Pisias, N.G., Roy, M., 2006. The middle Pleistocene
1002 transition: characteristics, mechanisms, and implications for long-term
1003 changes in atmospheric pCO₂. *Quaternary Science Reviews* 25, 3150–3184.
1004 doi:10.1016/j.quascirev.2006.07.008.
- 1005 Dakos, V., Scheffer, M., van Nes, E.H., Brovkin, V., Petoukhov, V., Held, H.,
1006 2008. Slowing down as an early warning signal for abrupt climate change.
1007 *Proceedings of the National Academy of Sciences* 105, 14308–14312.

- 1008 Dansgaard, W., Johnsen, S.J., Clausen, H.B., Dahl-Jensen, D., Gundestrup,
1009 N.S., Hammer, C.U., Hvidberg, C.S., Steffensen, J.P., Sveinbjörnsdóttir,
1010 A.E., Jouzel, J., Bond, G., 1993. Evidence for general instability of past
1011 climate from a 250-kyr ice-core record. *Nature* 364, 218–220. doi:10.1038/
1012 364218a0.
- 1013 deMenocal, P.B., 1995. Plio-pleistocene african climate. *Science* 270, 53–59.
1014 doi:10.1126/science.270.5233.53.
- 1015 DeMenocal, P.B., 2004. African climate change and faunal evolution during
1016 the Pliocene–Pleistocene. *Earth and Planetary Science Letters* 220, 3–24.
1017 doi:10.1016/S0012-821X(04)00003-2.
- 1018 Donges, J.F., Donner, R.V., Kurths, J., 2013. Testing time series irreversibil-
1019 ity using complex network methods. *EPL (Europhysics Letters)* 102, 10004.
1020 doi:10.1209/0295-5075/102/10004.
- 1021 Donges, J.F., Donner, R.V., Marwan, N., Breitenbach, S.F.M., Rehfeld, K.,
1022 Kurths, J., 2015a. Non-linear regime shifts in Holocene Asian monsoon
1023 variability: potential impacts on cultural change and migratory patterns.
1024 *Climate of the Past* 11, 709–741. doi:10.5194/cp-11-709-2015.
- 1025 Donges, J.F., Donner, R.V., Rehfeld, K., Marwan, N., Trauth, M.H., Kurths,
1026 J., 2011a. Identification of dynamical transitions in marine palaeoclimate
1027 records by recurrence network analysis. *Nonlinear Processes in Geophysics*
1028 18, 545–562. doi:10.5194/npg-18-545-2011.
- 1029 Donges, J.F., Donner, R.V., Trauth, M.H., Marwan, N., Schellnhuber, H.J.,
1030 Kurths, J., 2011b. Nonlinear detection of paleoclimate-variability transi-
1031 tions possibly related to human evolution. *Proceedings of the National*
1032 *Academy of Sciences* 108, 20422–20427. doi:10.1073/pnas.1117052108.
- 1033 Donges, J.F., Heitzig, J., Beronov, B., Wiedermann, M., Runge, J., Feng,
1034 Q.Y., Tupikina, L., Stolbova, V., Donner, R.V., Marwan, N., Dijkstra,
1035 H.A., Kurths, J., 2015b. Unified functional network and nonlinear time
1036 series analysis for complex systems science: The pyunicorn package. *Chaos*
1037 25, 113101. doi:10.1063/1.4934554.
- 1038 Donner, R.V., Heitzig, J., Donges, J.F., Zou, Y., Marwan, N., Kurths, J.,
1039 2011. *The Geometry of Chaotic Dynamics – A Complex Network Per-*

- 1040 spectively. *European Physical Journal B* 84, 653–672. doi:10.1140/epjb/
1041 e2011-10899-1.
- 1042 Donner, R.V., Zou, Y., Donges, J.F., Marwan, N., Kurths, J., 2010. Recur-
1043 rence networks – A novel paradigm for nonlinear time series analysis. *New*
1044 *Journal of Physics* 12, 033025. doi:10.1088/1367-2630/12/3/033025.
- 1045 Eckmann, J.P., Ruelle, D., 1992. Fundamental limitations for estimating
1046 dimensions and Lyapunov exponents in dynamical systems. *Physica D* 56,
1047 185–187. doi:10.1016/0167-2789(92)90023-G.
- 1048 Eroglu, D., McRobie, F.H., Ozken, I., Stemler, T., Wyrwoll, K.H., Breiten-
1049 bach, S.F.M., Marwan, N., Kurths, J., 2016. See-saw relationship of the
1050 Holocene East Asian-Australian summer monsoon. *Nature Communica-*
1051 *tions* 7, 12929. doi:10.1038/ncomms12929.
- 1052 Fan, J., Meng, J., Ludescher, J., Chen, X., Ashkenazy, Y., Kurths, J., Havlin,
1053 S., Schellnhuber, H.J., 2021. Statistical physics approaches to the complex
1054 Earth system. *Physics Reports* 896, 1–84. doi:10.1016/j.physrep.2020.
1055 09.005.
- 1056 Feldhoff, J.H., Donner, R.V., Donges, J.F., Marwan, N., Kurths, J., 2012.
1057 Geometric detection of coupling directions by means of inter-system re-
1058 currence networks. *Physics Letters A* 376, 3504–3513. doi:10.1016/j.
1059 physleta.2012.10.008.
- 1060 Friedrich, R., Peinke, J., Sahimi, M., Reza Rahimi Tabar, M., 2011. Ap-
1061 proaching complexity by stochastic methods: From biological systems to
1062 turbulence. *Physics Reports* 506, 87–162. doi:10.1016/j.physrep.2011.
1063 05.003.
- 1064 Gao, Z.K., Cai, Q., Yang, Y.X., Dang, W.D., Zhang, S.S., 2016. Multiscale
1065 limited penetrable horizontal visibility graph for analyzing nonlinear time
1066 series. *Scientific Reports* 6, 35622. doi:10.1038/srep35622.
- 1067 Gapelyuk, A., Schirdewan, A., Fischer, R., Wessel, N., 2010. Cardiac mag-
1068 netic field mapping quantified by Kullback–Leibler entropy detects patients
1069 with coronary artery disease. *Physiological Measurement* 31, 1345–1354.
1070 doi:10.1088/0967-3334/31/10/004.

- 1071 Gardiner, C., 2009. *Stochastic Methods – A Handbook for the Natural and*
1072 *Social Sciences*. Springer Berlin Heidelberg, Berlin, Heidelberg.
- 1073 Garland, J., Jones, T., Neuder, M., Morris, V., White, J., Bradley, E., 2018.
1074 *Anomaly Detection in Paleoclimate Records Using Permutation Entropy*.
1075 *Entropy* 20, 931. doi:10.3390/e20120931.
- 1076 Gershenfeld, N.A., 1992. Dimension measurement on high-dimensional sys-
1077 tems. *Physica D: Nonlinear Phenomena* 55, 135–154. doi:10.1016/
1078 0167-2789(92)90193-Q.
- 1079 Ghil, M., 2002. Advanced spectral methods for climatic time series. *Reviews*
1080 *of Geophysics* 40, 1003. doi:10.1029/2000RG000092.
- 1081 Goswami, B., Boers, N., Rheinwalt, A., Marwan, N., Heitzig, J., Breitenbach,
1082 S.F.M., Kurths, J., 2018. Abrupt transitions in time series with uncertain-
1083 ties. *Nature Communications* 9, 48. doi:10.1038/s41467-017-02456-6.
- 1084 Goswami, B., Marwan, N., Feulner, G., Kurths, J., 2013. How do global
1085 temperature drivers influence each other? – A network perspective using
1086 recurrences. *European Physical Journal – Special Topics* 222, 861–873.
1087 doi:10.1140/epjst/e2013-01889-8.
- 1088 Grassberger, P., 1986. Do climatic attractors exist? *Nature* 323, 609–612.
1089 doi:10.1038/323609a0.
- 1090 Grassberger, P., Procaccia, I., 1983. Measuring the strangeness of strange
1091 attractors. *Physica D* 9, 189–208. doi:10.1016/0167-2789(83)90298-1.
- 1092 Grassberger, P., Procaccia, I., 1984. Dimensions and entropies of strange
1093 attractors from a fluctuating dynamics approach. *Physics Letters A* 13,
1094 34–54. doi:10.1016/0167-2789(84)90269-0.
- 1095 Han, W., Appel, E., Galy, A., Rösler, W., Fang, X., Zhu, X., Vanden-
1096 berghe, J., Wang, J., Berger, A., Lü, S., Zhang, T., 2020. Climate
1097 transition in the Asia inland at 0.8–0.6 Ma related to astronomically
1098 forced ice sheet expansion. *Quaternary Science Reviews* 248, 106580.
1099 doi:10.1016/j.quascirev.2020.106580.
- 1100 Hannisdal, B., 2011. Non-parametric inference of causal interactions from
1101 geological records. *American Journal of Science* 311, 315–334. doi:10.
1102 2475/04.2011.02.

- 1103 Hassanibesheli, F., Boers, N., Kurths, J., 2020. Reconstructing complex
1104 system dynamics from time series: a method comparison. *New Journal of*
1105 *Physics* 22, 073053. doi:10.1088/1367-2630/ab9ce5.
- 1106 Haug, G.H., Tiedemann, R., 1998. Effect of the formation of the Isthmus of
1107 Panama on Atlantic Ocean thermohaline circulation. *Nature* 393, 673–676.
1108 doi:10.1038/31447.
- 1109 Herbert, T.D., Peterson, L.C., Lawrence, K.T., Liu, Z., 2010. Tropical Ocean
1110 Temperatures Over the Past 3.5 Million Years. *Science* 328, 1530–1534.
1111 doi:10.1126/science.1185435.
- 1112 Hughes, T.P., Carpenter, S., Rockström, J., Scheffer, M., Walker, B., 2013.
1113 Multiscale regime shifts and planetary boundaries. *Trends in ecology &*
1114 *evolution* 28, 389–395.
- 1115 Kantz, H., 1994. Quantifying the closeness of fractal measures. *Physical*
1116 *Review E* 49, 5091–5097. doi:10.1103/PhysRevE.49.5091.
- 1117 Kantz, H., Schreiber, T., 1997. *Nonlinear Time Series Analysis*. University
1118 Press, Cambridge.
- 1119 Kennel, M.B., Brown, R., Abarbanel, H.D.I., 1992. Determining embedding
1120 dimension for phase-space reconstruction using a geometrical construction.
1121 *Physical Review A* 45, 3403–3411. doi:10.1103/PhysRevA.45.3403.
- 1122 Kraemer, K.H., Datsoris, G., Kurths, J., Kiss, I.Z., Ocampo-Espindola, J.L.,
1123 Marwan, N., 2021. A unified and automated approach to attractor recon-
1124 struction. *New Journal of Physics* 23, 033017. doi:10.1088/1367-2630/
1125 abe336.
- 1126 Kraemer, K.H., Donner, R.V., Heitzig, J., Marwan, N., 2018. Recurrence
1127 threshold selection for obtaining robust recurrence characteristics in dif-
1128 ferent embedding dimensions. *Chaos* 28, 085720. doi:10.1063/1.5024914.
- 1129 Kwasniok, F., Lohmann, G., 2009. Deriving dynamical models from paleo-
1130 climatic records: Application to glacial millennial-scale climate variability.
1131 *Physical Review E* 80, 1–9. doi:10.1103/PhysRevE.80.066104.

- 1132 Kwasniok, F., Lohmann, G., 2012. A stochastic nonlinear oscillator
1133 model for glacial millennial-scale climate transitions derived from ice-
1134 core data. *Nonlinear Processes in Geophysics* 19, 595–603. doi:10.5194/
1135 npg-19-595-2012.
- 1136 Lacasa, L., Luque, B., Ballesteros, F., Luque, J., Nuño, J.C., 2008. From
1137 time series to complex networks: The visibility graph. *Proceedings of the*
1138 *National Academy of Sciences* 105, 4972. doi:10.1073/pnas.0709247105.
- 1139 Lacasa, L., Luque, B., Luque, J., Nuño, J.C., 2009. The visibility graph:
1140 A new method for estimating the Hurst exponent of fractional Brownian
1141 motion. *EPL (Europhysics Letters)* 86, 30001. doi:10.1209/0295-5075/
1142 86/30001.
- 1143 Lacasa, L., Nuñez, A., Roldán, É., Parrondo, J.M.R., Luque, B., 2012. Time
1144 series irreversibility: a visibility graph approach. *The European Physical*
1145 *Journal B* 85, 217. doi:10.1140/epjb/e2012-20809-8.
- 1146 Larrasoana, J.C., Roberts, A.P., Rohling, E.J., Winklhofer, M., Wehausen,
1147 R., 2003. Three million years of monsoon variability over the northern Sa-
1148 hara. *Climate Dynamics* 21, 689–698. doi:10.1007/s00382-003-0355-z.
- 1149 Lawrance, A.J., 1991. Directionality and Reversibility in Time Series. *Inter-*
1150 *national Statistical Review / Revue Internationale de Statistique* 59, 67.
1151 doi:10.2307/1403575.
- 1152 Lechleitner, F.A., Breitenbach, S.F.M., Cheng, H., Plessen, B., Rehfeld,
1153 K., Goswami, B., Marwan, N., Eroglu, D., Adkins, J., Haug, G., 2017.
1154 Climatic and in-cave influences on $\delta^{18}\text{O}$ and $\delta^{13}\text{C}$ in a stalagmite from
1155 northeastern India through the last deglaciation. *Quaternary Research* 88,
1156 458–471. doi:10.1017/qua.2017.72.
- 1157 Lekscha, J., Donner, R., 2020. Detecting dynamical anomalies in time se-
1158 ries from different palaeoclimate proxy archives using windowed recur-
1159 rence network analysis. *Nonlinear Processes in Geophysics* 27, 261–275.
1160 doi:10.5194/npg-27-261-2020.
- 1161 Lekscha, J., Donner, R.V., 2018. Phase space reconstruction for non-
1162 uniformly sampled noisy time series. *Chaos* 28, 085702. doi:10.1063/
1163 1.5023860.

- 1164 Lenton, T.M., Held, H., Kriegler, E., Hall, J.W., Lucht, W., Rahmstorf, S.,
1165 Schellnhuber, H.J., 2008. Tipping elements in the earth's climate system.
1166 Proceedings of the national Academy of Sciences 105, 1786–1793.
- 1167 Li, W.L., Zhong, W.Q., Jin, B.S., Xiao, R., He, T.T., 2013. Flow regime
1168 identification in a three-phase bubble column based on statistical, Hurst,
1169 Hilbert–Huang transform and Shannon entropy analysis. Chemical Engi-
1170 neering Science 102, 474–485. doi:10.1016/j.ces.2013.08.052.
- 1171 Lisiecki, L.E., 2010. Links between eccentricity forcing and the 100,000-year
1172 glacial cycle. Nature Geoscience 3, 349–352. doi:10.1038/ngeo828.
- 1173 Lisiecki, L.E., Raymo, M.E., 2005. A Pliocene-Pleistocene stack of 57 globally
1174 distributed benthic δ 18O records. Paleoceanography 20, 1–17. doi:10.
1175 1029/2004PA001071.
- 1176 Little, M.A., McSharry, P.E., Roberts, S.J., Costello, D.A.E., Moroz, I.M.,
1177 2007. Exploiting Nonlinear Recurrence and Fractal Scaling Properties for
1178 Voice Disorder Detection. Biomedical Engineering Online 6, 1–19. doi:10.
1179 1186/1475-925X-6-23.
- 1180 Livina, V., Ditlevsen, P., Lenton, T., 2012. An independent test of methods
1181 of detecting system states and bifurcations in time-series data. Physica A:
1182 Statistical Mechanics and its Applications 391, 485–496. doi:10.1016/j.
1183 physa.2011.08.025.
- 1184 Livina, V.N., Kwasniok, F., Lenton, T.M., 2010. Potential analysis reveals
1185 changing number of climate states during the last 60 kyr. Climate of the
1186 Past 6, 77–82. doi:10.5194/cp-6-77-2010.
- 1187 Livina, V.N., Kwasniok, F., Lohmann, G., Kantelhardt, J.W., Lenton, T.M.,
1188 2011. Changing climate states and stability: from Pliocene to present.
1189 Climate Dynamics 37, 2437–2453. doi:10.1007/s00382-010-0980-2.
- 1190 Lourens, L.J., Antonarakou, A., Hilgen, F.J., Van Hoof, A.A.M., Vergnaud-
1191 Grazzini, C., Zachariasse, W.J., 1996. Evaluation of the Plio-Pleistocene
1192 astronomical timescale. Paleoceanography 11, 391–413. doi:10.1029/
1193 96PA01125.

- 1194 Maasch, K.A., 1989. Calculating climate attractor dimension from $\delta^{18}\text{O}$
1195 records by the Grassberger-Procaccia algorithm. *Climate Dynamics* 4, 45–
1196 55. doi:10.1007/BF00207399.
- 1197 Malik, N., Marwan, N., Zou, Y., Mucha, P.J., Kurths, J., 2014. Fluctuation
1198 of similarity to detect transitions between distinct dynamical regimes in
1199 short time series. *Physical Review E* 89, 062908. doi:10.1103/PhysRevE.
1200 89.062908.
- 1201 Marwan, N., 2008. A Historical Review of Recurrence Plots. *Euro-
1202 pean Physical Journal – Special Topics* 164, 3–12. doi:10.1140/epjst/
1203 e2008-00829-1.
- 1204 Marwan, N., 2011. How to avoid potential pitfalls in recurrence plot based
1205 data analysis. *International Journal of Bifurcation and Chaos* 21, 1003–
1206 1017. doi:10.1142/S0218127411029008.
- 1207 Marwan, N., Donges, J.F., Zou, Y., Donner, R.V., Kurths, J., 2009. Complex
1208 network approach for recurrence analysis of time series. *Physics Letters A*
1209 373, 4246–4254. doi:10.1016/j.physleta.2009.09.042.
- 1210 Marwan, N., Kurths, J., 2015. Complex network based techniques to identify
1211 extreme events and (sudden) transitions in spatio-temporal systems. *Chaos*
1212 25, 097609. doi:10.1063/1.4916924.
- 1213 Marwan, N., Romano, M.C., Thiel, M., Kurths, J., 2007. Recurrence Plots for
1214 the Analysis of Complex Systems. *Physics Reports* 438, 237–329. doi:10.
1215 1016/j.physrep.2006.11.001.
- 1216 Marwan, N., Schinkel, S., Kurths, J., 2013. Recurrence plots 25 years later
1217 – gaining confidence in dynamical transitions. *Europhysics Letters* 101,
1218 20007. doi:10.1209/0295-5075/101/20007.
- 1219 Marwan, N., Trauth, M.H., Vuille, M., Kurths, J., 2003. Comparing modern
1220 and Pleistocene ENSO-like influences in NW Argentina using nonlinear
1221 time series analysis methods. *Climate Dynamics* 21, 317–326. doi:10.
1222 1007/s00382-003-0335-3.
- 1223 Marwan, N., Wessel, N., Meyerfeldt, U., Schirdewan, A., Kurths, J., 2002.
1224 Recurrence Plot Based Measures of Complexity and its Application to

- 1225 Heart Rate Variability Data. *Physical Review E* 66, 026702. doi:10.1103/
1226 PhysRevE.66.026702.
- 1227 Möller, M., Lange, W., Mitschke, F., Abraham, N., Hübner, U., 1989. Er-
1228 rors from digitizing and noise in estimating attractor dimensions. *Physics*
1229 *Letters A* 138, 176–182. doi:10.1016/0375-9601(89)90023-6.
- 1230 Mudelsee, M., Schulz, M., 1997. The Mid-Pleistocene climate transition:
1231 Onset of 100 ka cycle lags ice volume build-up by 280 ka. *Earth and*
1232 *Planetary Science Letters* 151, 117–123. doi:10.1016/S0012-821X(97)
1233 00114-3.
- 1234 Mudelsee, M., Stattegger, K., 1997. Exploring the structure of the mid-
1235 Pleistocene revolution with advanced methods of time-series analysis. *Ge-*
1236 *ologische Rundschau* 86, 499–511. doi:10.1007/s005310050157.
- 1237 Ozken, I., Eroglu, D., Stemler, T., Marwan, N., Bagci, G.B., Kurths, J., 2015.
1238 Transformation-cost time-series method for analyzing irregularly sampled
1239 data. *Physical Review E* 91, 062911. doi:10.1103/PhysRevE.91.062911.
- 1240 Packard, N.H., Crutchfield, J.P., Farmer, J.D., Shaw, R.S., 1980. Geometry
1241 from a Time Series. *Physical Review Letters* 45, 712–716. doi:10.1103/
1242 PhysRevLett.45.712.
- 1243 Pessa, A.A.B., Ribeiro, H.V., 2021. ordpy: A Python package for data
1244 analysis with permutation entropy and ordinal network methods. *Chaos*
1245 31, 063110. doi:10.1063/5.0049901.
- 1246 Petrick, B., Martínez-García, A., Auer, G., Reuning, L., Auderset, A.,
1247 Deik, H., Takayanagi, H., De Vleeschouwer, D., Iryu, Y., Haug, G.H.,
1248 2019. Glacial Indonesian Throughflow weakening across the Mid-
1249 Pleistocene Climatic Transition. *Scientific Reports* 9, 16995. doi:10.1038/
1250 s41598-019-53382-0.
- 1251 Potts, R., 1996. Evolution and Climate Variability. *Science* 273, 922–923.
1252 doi:10.1126/science.273.5277.922.
- 1253 Prasad, S., Marwan, N., Eroglu, D., Goswami, B., Mishra, P.K., Gaye, B.,
1254 Anoop, A., Basavaiah, N., Stebich, M., Jehangir, A., 2020. Holocene
1255 climate forcings and lacustrine regime shifts in the Indian summer monsoon

- 1256 realm. *Earth Surface Processes and Landforms* 45, 3842–3853. doi:10.
1257 1002/esp.5004.
- 1258 Ravelo, A.C., Andreasen, D.H., Lyle, M., Olivarez Lyle, A., Wara, M.W.,
1259 2004. Regional climate shifts caused by gradual global cooling in the
1260 Pliocene epoch. *Nature* 429, 263–267. doi:10.1038/nature02567.
- 1261 Rawald, T., Sips, M., Marwan, N., 2017. PyRQA – Conducting Recurrence
1262 Quantification Analysis on Very Long Time Series Efficiently. *Computers
1263 & Geosciences* 104, 101–108. doi:10.1016/j.cageo.2016.11.016.
- 1264 Rehfeld, K., Marwan, N., Breitenbach, S.F.M., Kurths, J., 2013. Late
1265 Holocene Asian summer monsoon dynamics from small but complex net-
1266 works of paleoclimate data. *Climate Dynamics* 41, 3–19. doi:10.1007/
1267 s00382-012-1448-3.
- 1268 Rehfeld, K., Marwan, N., Heitzig, J., Kurths, J., 2011. Comparison of cor-
1269 relation analysis techniques for irregularly sampled time series. *Nonlinear
1270 Processes in Geophysics* 18, 389–404. doi:10.5194/npg-18-389-2011.
- 1271 Richman, J.S., Moorman, J.R., 2000. Physiological time-series analysis using
1272 approximate entropy and sample entropy. *American Journal of Physiology
1273 – Heart and Circulatory Physiology* 278, H2039–H2049.
- 1274 Risken, H., 1989. The Fokker-Planck Equation. volume 18 of *Springer Series
1275 in Synergetics*. Springer Berlin Heidelberg, Berlin, Heidelberg. doi:10.
1276 1007/978-3-642-61544-3.
- 1277 Rocha, J.C., Peterson, G., Bodin, Ö., Levin, S., 2018. Cascading regime
1278 shifts within and across scales. *Science* 362, 1379–1383.
- 1279 Rockström, J., Steffen, W., Noone, K., Persson, Å., Chapin, F.S., Lambin,
1280 E.F., Lenton, T.M., Scheffer, M., Folke, C., Schellnhuber, H.J., et al., 2009.
1281 A safe operating space for humanity. *nature* 461, 472–475.
- 1282 Rosenstein, M.T., Collins, J.J., De Luca, C.J., 1993. A practical method for
1283 calculating largest Lyapunov exponents from small data sets. *Physica D:
1284 Nonlinear Phenomena* 65, 117–134. doi:10.1016/0167-2789(93)90009-P.
- 1285 Sauramo, M., 1918. Geochronologische studien über die spätglaziale zeit in
1286 südfinnland. *Bulletin de la Commission Géologique de Finlande* 50, 3–48.

- 1287 Scheffer, M., Bascompte, J., Brock, W.A., Brovkin, V., Carpenter, S.R.,
1288 Dakos, V., Held, H., Van Nes, E.H., Rietkerk, M., Sugihara, G., 2009.
1289 Early-warning signals for critical transitions. *Nature* 461, 53–59.
- 1290 Scheffer, M., Carpenter, S.R., 2003. Catastrophic regime shifts in ecosystems:
1291 linking theory to observation. *Trends in ecology & evolution* 18, 648–656.
- 1292 Schellnhuber, H.J., 2009. Tipping elements in the earth system. *Proceedings*
1293 *of the National Academy of Sciences* 106, 20561–20563.
- 1294 Schleussner, C.F., Divine, D.V., Donges, J.F., Miettinen, A., Donner, R.V.,
1295 2015. Indications for a North Atlantic ocean circulation regime shift at
1296 the onset of the Little Ice Age. *Climate Dynamics* 45, 3623–3633. doi:10.
1297 1007/s00382-015-2561-x.
- 1298 Schölzel, C., Friederichs, P., 2008. Multivariate non-normally distributed
1299 random variables in climate research – introduction to the copula ap-
1300 proach. *Nonlinear Processes in Geophysics* 15, 761–772. doi:10.5194/
1301 npg-15-761-2008.
- 1302 Schulz, M., Mudelsee, M., Wolf-Welling, T., 1994. Fractal Analyses of Pleis-
1303 tocene Marine Oxygen Isotope Records, in: *Fractals and Dynamic Systems*
1304 *in Geoscience*. Springer, Berlin Heidelberg, p. 377–387.
- 1305 Schütz, N., Holschneider, M., 2011. Detection of trend changes in time series
1306 using Bayesian inference. *Physical Review E* 84, 021120. doi:10.1103/
1307 PhysRevE.84.021120.
- 1308 Shannon, C., 1948. A mathematical theory of communication. *Bell System*
1309 *Technical Journal*, The 27, 379–423. doi:10.1002/j.1538-7305.1948.
1310 tb01338.x.
- 1311 Silverman, B.W., 1986. *Density Estimation for Statistics and Data Analysis*.
1312 volume 26. CRC Press.
- 1313 Singh, M., Krishnan, R., Goswami, B., Choudhury, A.D., Swapna, P.,
1314 Vellore, R., Prajeesh, A.G., Sandeep, N., Venkataraman, C., Donner,
1315 R.V., Marwan, N., Kurths, J., 2020. Fingerprint of volcanic forcing
1316 on the ENSO–Indian monsoon coupling. *Science Advances* 6, eaba8164.
1317 doi:10.1126/sciadv.aba8164.

- 1318 Smirnov, D.A., Marwan, N., Breitenbach, S.F.M., Lechleitner, F., Kurths,
1319 J., 2017. Coping with dating errors in causality estimation. *Europhysics*
1320 *Letters* 117, 10004. doi:10.1209/0295-5075/117/10004.
- 1321 Spiridonov, A., Balakauskas, L., Stankevic, R., Kluczynska, G., Gedminiene,
1322 L., Stancikaite, M., 2019. Holocene vegetation patterns in southern Lithua-
1323 nia indicate astronomical forcing on the millennial and centennial time
1324 scales. *Scientific Reports* 9, 14711. doi:10.1038/s41598-019-51321-7.
- 1325 Spiridonov, A., Stankevič, R., Gečas, T., Brazauskas, A., Kaminskas, D.,
1326 Musteikis, P., Kaveckas, T., Meidla, T., Bičkauskas, G., Ainsaar, L.,
1327 Radzevičius, S., 2020. Ultra-high resolution multivariate record and mul-
1328 tiscala causal analysis of Pridoli (late Silurian): Implications for global
1329 stratigraphy, turnover events, and climate-biota interactions. *Gondwana*
1330 *Research* 86, 222–249. doi:10.1016/j.gr.2020.05.015.
- 1331 Spiridonov, A., Vaikutienė, G., Stankevič, R., Druzhinina, O., Šeirienė, V.,
1332 Subetto, D., Kublitsky, J., Stančikaitė, M., 2021. Response of freshwater
1333 diatoms to cold events in the Late Pleistocene and Early Holocene (SE
1334 Baltic region). *Quaternary International* 589, 112–123. doi:10.1016/j.
1335 *quaint*.2021.02.017.
- 1336 Stanley, D.J., 1978. Ionian Sea sapropel distribution and late Quaternary
1337 palaeoceanography in the eastern Mediterranean. *Nature* 274, 149.
- 1338 Staubwasser, M., Weiss, H., 2006. Holocene climate and cultural evolution
1339 in late prehistoric–early historic West Asia. *Quaternary Research* 66, 372–
1340 387. doi:10.1016/j.yqres.2006.09.001.
- 1341 Steffen, W., Richardson, K., Rockström, J., Cornell, S.E., Fetzer, I., Bennett,
1342 E.M., Biggs, R., Carpenter, S.R., De Vries, W., De Wit, C.A., et al., 2015.
1343 Planetary boundaries: Guiding human development on a changing planet.
1344 *Science* 347.
- 1345 Steffen, W., Rockström, J., Richardson, K., Lenton, T.M., Folke, C., Liv-
1346 erman, D., Summerhayes, C.P., Barnosky, A.D., Cornell, S.E., Crucifix,
1347 M., et al., 2018. Trajectories of the earth system in the anthropocene.
1348 *Proceedings of the National Academy of Sciences* 115, 8252–8259.

- 1349 Supriya, S., Siuly, S., Wang, H., Cao, J., Zhang, Y., 2016. Weighted Visibility
1350 Graph With Complex Network Features in the Detection of Epilepsy. IEEE
1351 Access 4, 6554–6566. doi:10.1109/ACCESS.2016.2612242.
- 1352 Takens, F., 1981. Detecting Strange Attractors in Turbulence, in: Rand, D.,
1353 Young, L.S. (Eds.), Dynamical Systems and Turbulence. Springer, Berlin.
1354 volume 898 of *Lecture Notes in Mathematics*, pp. 366–381.
- 1355 Theiler, J., Eubank, S., Longtin, A., Galdrikian, B., Farmer, B., 1992. Test-
1356 ing for nonlinearity in time series: the method of surrogate data. *Physica*
1357 *D* 58, 77–94. doi:10.1016/0167-2789(92)90102-S.
- 1358 Thiel, M., Romano, M.C., Read, P.L., Kurths, J., 2004. Estimation of dy-
1359 namical invariants without embedding by recurrence plots. *Chaos* 14, 234–
1360 243. doi:10.1063/1.1667633.
- 1361 Tiedemann, R., Sarnthein, M., Shackleton, N.J., 1994. Astronomic timescale
1362 for the Pliocene Atlantic $\delta^{18}\text{O}$ and dust flux records of Ocean Drilling
1363 Program site 659. *Paleoceanography* 9, 619–638.
- 1364 Trauth, M.H., 2005. Late Cenozoic Moisture History of East Africa. *Science*
1365 309, 2051–2053. doi:10.1126/science.1112964.
- 1366 Trauth, M.H., 2021. Spectral Analysis in Quaternary Sciences. *Quaternary*
1367 *Science Reviews* 270, 107157. doi:10.1016/j.quascirev.2021.107157.
- 1368 Trauth, M.H., Asrat, A., Cohen, A.S., Duesing, W., Foerster, V., Kaboth-
1369 Bahr, S., Kraemer, K.H., Lamb, H.F., Marwan, N., Maslin, M.A.,
1370 Schäbitz, F., 2021. Recurring types of variability and transitions in the
1371 ~ 620 kyr record of climate change from the Chew Bahir basin, south-
1372 ern Ethiopia. *Quaternary Science Reviews* 266, 106777. doi:10.1016/j.
1373 quascirev.2020.106777.
- 1374 Trauth, M.H., Larrasoña, J.C., Mudelsee, M., 2009. Trends, rhythms and
1375 events in plio-pleistocene african climate. *Quaternary Science Reviews* 28,
1376 399–411. doi:10.1016/j.quascirev.2008.11.003.
- 1377 Vautard, R., Ghil, M., 1989. Singular spectrum analysis in nonlinear dynam-
1378 ics, with applications to paleoclimatic time series. *Physica D: Nonlinear*
1379 *Phenomena* 35, 395–424. doi:10.1016/0167-2789(89)90077-8.

- 1380 Voss, H., Kurths, J., Schwarz, U., 1996. Reconstruction of grand minima
1381 of solar activity from radiocarbon data. *Journal of Geophysical Research*
1382 101, 15637–15643. doi:10.1029/96JA00542.
- 1383 Webber, Jr., C.L., Marwan, N., Facchini, A., Giuliani, A., 2009. Simpler
1384 methods do it better: Success of Recurrence Quantification Analysis as
1385 a general purpose data analysis tool. *Physics Letters A* 373, 3753–3756.
1386 doi:10.1016/j.physleta.2009.08.052.
- 1387 Westerhold, T., Marwan, N., Drury, A.J., Liebrand, D., Agnini, C., Anag-
1388 nostou, E., Barnet, J.S.K., Bohaty, S.M., De Vleeschouwer, D., Florindo,
1389 F., Frederichs, T., Hodell, D.A., Holbourn, A.E., Kroon, D., Laurentano,
1390 V., Littler, K., Lourens, L.J., Lyle, M., Pälike, H., Röhl, U., Tian, J.,
1391 Wilkens, R.H., Wilson, P.A., Zachos, J.C., 2020. An astronomically dated
1392 record of Earth’s climate and its predictability over the last 66 million
1393 years. *Science* 369, 1383–1387. doi:10.1126/science.aba6853.
- 1394 Wolf, A., Swift, J.B., Swinney, H.L., Vastano, J.A., 1985. Determin-
1395 ing Lyapunov Exponents from a Time Series. *Physica D* 16, 285–317.
1396 doi:10.1016/0167-2789(85)90011-9.
- 1397 Zanin, M., Olivares, F., 2021. Ordinal patterns-based methodologies for
1398 distinguishing chaos from noise in discrete time series. *Communications*
1399 *Physics* 4, 190. doi:10.1038/s42005-021-00696-z.
- 1400 Zbilut, J.P., Webber, Jr., C.L., 2007. Recurrence quantification analysis:
1401 Introduction and historical context. *International Journal of Bifurcation*
1402 *and Chaos* 17, 3477–3481. doi:10.1142/S0218127407019238.
- 1403 Zhao, X., Ji, M., Zhang, N., Shang, P., 2020. Permutation transition entropy:
1404 Measuring the dynamical complexity of financial time series. *Chaos, Soli-*
1405 *tons & Fractals* 139, 109962. doi:10.1016/j.chaos.2020.109962.
- 1406 Zou, Y., Donner, R., Marwan, N., Small, M., Kurths, J., 2014. Long-term
1407 changes in the north-south asymmetry of solar activity: A nonlinear dy-
1408 namics characterization using visibility graphs. *Nonlinear Processes in*
1409 *Geophysics* 21. doi:10.5194/npg-21-1113-2014.
- 1410 Zou, Y., Donner, R.V., Donges, J.F., Marwan, N., Kurths, J., 2010. Identify-
1411 ing complex periodic windows in continuous-time dynamical systems using
1412 recurrence-based methods. *Chaos* 20, 043130. doi:10.1063/1.3523304.

1413 Zou, Y., Donner, R.V., Marwan, N., Donges, J.F., Kurths, J., 2019. Complex
1414 network approaches to nonlinear time series analysis. *Physics Reports* 787,
1415 1–97. doi:10.1016/j.physrep.2018.10.005.